Advances in Optics and Photonics

Filtering light with nanoparticles: a review of optically selective particles and applications

TODD P. OTANICAR,[1,*] DREW DEJARNETTE,[1] YASITHA HEWAKURUPPU,[2] AND ROBERT A. TAYLOR[2]

[1]Department of Mechanical Engineering, The University of Tulsa, 800 South Tucker Drive, Tulsa, Oklahoma 74104, USA
[2]School of Mechanical and Manufacturing Engineering, University of New South Wales, Sydney, NSW 2052, Australia
*Corresponding author: todd-otanicar@utulsa.edu

Received May 4, 2016; revised August 5, 2016; accepted August 9, 2016; published September 2, 2016 (Doc. ID 264549)

The ability to selectively and controllably interact with light is useful to a wide range of devices. With the advent of nanotechnology, we now have the ability to create optical materials, which are designed from the bottom up, with dimensions of the order of the wavelength of light. While it has been known for some time that nanoparticles exhibit such exciting properties, recent (widespread) research in nanoparticles has significantly increased our understanding of how to fabricate and use nanoparticles for a myriad of enduring and emerging optical applications. Drastic modifications to the "bulk" optical properties of standard materials in these applications are possible, enabling "nano-engineered" optical properties with several degrees of design freedom, including material, size, morphology, surrounding media, and nearby structures. Understanding these sensitivities has led to optical control from the ultraviolet through the infrared spectrum. To highlight this, the following review provides a comprehensive snapshot of how these effects have been captured in models and experimentally demonstrated in terms of spectral selectivity in absorption, scattering, and emission. In addition, we discuss recent progress toward using nanoparticles in real applications, most commonly in fluid suspensions or solid thin films as a means to create the next generation of highly scalable and (potentially) low-cost spectrally selective optical materials.

OCIS codes: (230.7408) Wavelength filtering devices; (250.5403) Plasmonics; (290.0290) Scattering; (350.5340) Photothermal effects; (350.6050) Solar energy
http://dx.doi.org/10.1364/AOP.8.000541

Filtering light with nanoparticles: a review of optically selective particles and applications

Todd P. Otanicar, Drew DeJarnette, Yasitha Hewakuruppu, and Robert A. Taylor

1. INTRODUCTION

Control of light–matter interactions on the nanoscale has led to the ability to design new large-scale devices and add functionality to existing devices. Since most materials interact with light only over a specific band of incident energies, and these interactions are altered when the dimension of the material becomes comparable to the wavelength of light, it is possible to obtain nano-engineered materials that enhance our ability to control light. Advances in materials fabrication techniques have enabled bespoke nano-materials that can be tuned to absorb unwanted or damaging wavelengths, selectively transmit and/or reflect desired portions of the incident spectrum, and/or spatially redirect portions of the spectrum. Figure 1 presents a simplified schematic of these optical interactions. Some of these approaches have been historically used in optical equipment for spectroscopy [1], but recently have been scaled to solar energy applications [2–5].

Selective absorption can be achieved relatively easily through the addition of impurities to transparent glasses/plastics. The impurities can be molecular dyes, paints, or small particles—as we will highlight in more detail below—made from various inorganic or organic compounds. In order to filter light, these compounds need only to be selective about which wavelengths they absorb and transmit through the base transparent material. Inks, stained glasses, and colored plastics represent the many ubiquitous examples of absorbing filters [6]. Prior to modern nanostructure synthesis methods, the creation of absorption filters was limited to an empirical mix and measure approach with little ability to control the underlying physics (although nanomaterials were sometimes involved—e.g., the Lycurgus Cup).

Selective emission, or photoluminescence, also typically relies on absorption of incident light—typically ultraviolet (UV) or visible light—to excite the nanoparticle or a dye molecule (fluorescence) attached to the nanoparticle. When the excited state decays, a photon will be emitted at a lower energy level than the originally absorbed light. Aside from its many uses in biology, chemistry, and lighting, fluorescence can be used to downconvert (or even upconvert) sunlight [7–9]. While spectral conversion remains a promising approach to fully utilize the entire solar spectrum, it is limited by a small wavelength range for absorption and re-emission, as well as low quantum efficiencies.

Selective transmission and reflection is primarily achieved through the use of thin-film coatings, often behaving as interferometers. Interferometers are a class of optical devices in which the incident beam is superimposed either with itself or with a reference beam in a way that enables the propagation of light to be controlled. As the most widely used basis for this purpose, the Charles Fabry and Alfred Perot "amplitude splitting" interferometer [10] consists of a pair of partially reflecting mirrors in which multiple reflections of light create interference fringes that can be used to analyze (or control) the spectral properties of light propagating through the system. This basic

structure has been refined further to create dichroic thin films in which several pairs of high and low refractive index thin films are deposited onto a substrate to selectively reflect and transmit the desired wavelengths of light. (Note: This is also sometimes referred to as a distributed Bragg reflector when layers of alternating materials are embedded inside a waveguide material). Spectral selection is achieved in this instance by constructive interference of light, which partially reflects off layers that are roughly one-fourth the thickness of the desired incident wavelength. If several of these layers are placed in series, the resulting dichroic mirror can be designed to have anything from a simple edge-pass to a multiple bandpass nature. Their effective optical properties are controlled by the materials, number of layers, and thickness of the layers used [11]. Applications of dichroic-type filters range from optical metrology equipment to spectrally selective mirrors, and surfaces for "splitting" of incident solar energy [3,4,11–13]. Recently, thin-film structures have been shown to create passive cooling below ambient temperatures through high emissivity in the sky window and high solar reflectance [14]. In addition to more conventional layered thin films, the ability to create surface structures of the order of the wavelength of light on a thin film/substrate is creating new possibilities for further control. A wide variety of structures are available to achieve this, as noted in some recent reviews [15–17]. One approach has been the combination of pillars and pyramids coupled with a conventional thin film for selective reflection and radiative cooling of a surface [18]. Others are pursuing the creation of spectrally selective surfaces for solar thermal collectors [19,20] or selective absorber/emitters for thermophotovoltaic applications [21]. As we will show below, many of these types of coatings are being created with or enhanced by the integration of nanoparticles into the coating materials, or as the coatings themselves.

As an alternative to selective absorption and selective reflection, spectral redirection represents another method for more effectively utilizing light. While selective reflection can also be considered redirection, by this we mean devices that are designed specifically to spatially separate spectral bands. These types of devices have often been proposed for concentrating photovoltaic (CPV) applications in which cells of different bandgaps are stacked laterally, as opposed to the conventional multijunction cell (which is stacked vertically), using diffractive optics [22,23]. Other approaches are luminescent solar concentrators in which selective elements absorb and remit radiation preferentially in one direction [24,25]. Another approach, although less widely explored, is the use of holographic elements for spectral beam splitting, in which the incoming light can be broken into spectral components spatially [23,26].

As briefly demonstrated in this introduction, there are several modern approaches to split (via selective reflection) or filtered (via selective absorption) light at nearly any desired wavelength. With few exceptions, these are generally solid substrates that are

Figure 1

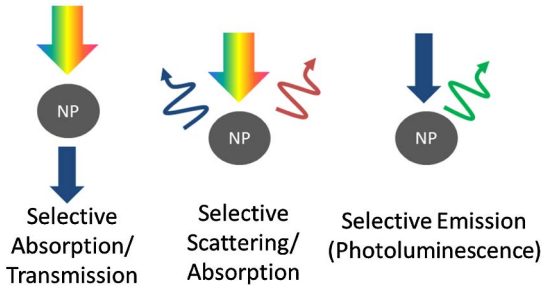

Schematic of optically selective nanoparticles.

produced only on the mm^2 to cm^2 scale. Many of these techniques, such as upconversion and downconversion, are limited to laboratory scale applications. Thin-film and doped-glass technologies have been demonstrated and are commercially available on scales facilitating use in devices on the large scale. Off-the-shelf costs of some of these devices are of the order of $100,000–500,000$ USD$/m^2$ for dichroic filters and $20,000–40,000$ USD$/m^2$ for doped glasses from optical component suppliers (such as Edmond Optics and Semrock).

While many of the technologies mentioned above have their own review articles, this paper will focus on the newest approach to spectral filtration, e.g., those based upon nanoparticles. Nanoparticles, unlike solid substrate approaches, are not limited to being embedded in or on solid substrates, but can also be suspended in fluids, which creates the potential for dynamic changes in their optical properties over time. While there exist a number of papers that have reviewed the properties and synthesis of nanoparticles in applications such as energy, medicine, electronics, and sensors, to our knowledge no such review exists that focuses on the optical properties of nanoparticles for optical filtration. It should be noted that Cortie and McDonagh have a thorough review of plasmonic nanoparticles (specifically gold and silver, including alloys with copper and aluminum), with a focus on synthesis, optical properties, and a limited investigation of applications [27]. In particular, this paper focuses on nanoparticles that are either embedded in nonparticipating (or mildly participating) media or arranged on a surface but still identifiably nanoparticles. A specific emphasis, although not exclusive, is placed on nanoparticles that utilize surface electron oscillation, called plasmons, to absorb select wavelengths of light depending on the nanoparticle size, shape, and composition. We believe this class of technology has more potential to be scaled up to the m^2 (or even km^2) sized application of solar energy systems and focus on applications where the primary goal is selective absorption or scattering of solar irradiance.

2. THEORETICAL BACKGROUND

Spectral absorption and scattering for metal spheres was described analytically by Gustov Mie in 1908 [28]. As such, a complete solution exists to determine the optical properties of spherical nanoparticles of arbitrary size. However, there are several underlying assumptions used by Mie in the derivation that call for alternative methods to calculate the optical properties of a nanoparticle. Additionally, Mie theory applies to the optical properties of only a single isolated nanoparticle in a homogeneous background. Several circumstances require knowledge of the effects on the optical properties of interacting nanoparticles or nanoparticles at an interface where Mie theory does not apply. Furthermore, treatment of the nanoparticles as dipoles provides insights into the physical mechanisms behind the optical properties, as opposed to performing numerical simulations that have higher accuracy but obscure phenomenological effects.

2.1. Dipole Modeling

A nanoparticle has the ability to confine waves to its surface through the process called plasmon oscillation. A plasmon is a surface wave of electrons that exists at the interface between two materials through which the real component of the complex dielectric function changes sign. Since most media have positive dielectric functions, plasmon resonance is limited to materials with a high number of free carriers, such as metals or highly doped semiconducting nanocrystals. Plasmon resonance is observed only for thin films or nanoscale structures since bulk properties dominate for particles larger than approximately 500 nm. Additionally, surface modes quickly become complicated due to multiple interactions for larger particle sizes.

When a photon hits a nanoparticle it forces the electrons to oscillate. If the frequency of light is near the natural oscillation frequency for the electrons, a significant portion of the light energy can be converted to the plasmon oscillation. Once excited, the plasmon decays in a matter of picoseconds into either absorption (phonon) or scattering (photon). Other forms of plasmon decay include hot electron transfer, which occurs through interactions between nanoparticles and bulk materials [29].

Nanoparticle absorption and scattering have wide application in sensing, waveguiding, electronics, and light filtration. Particles much smaller than the incident wavelength of light can be treated as dipoles. Light incident on a dipole induces electron oscillation, causing radiation. Larger particles induce higher order electric modes, such as quadrupoles. As a result, the scattering profile of light from nanoparticles is modal with the primary source of scattered light for small particles being dipolar in nature. Taking advantage of this scattering profile has lead researchers to create photonic crystals to control the coupling interactions between adjacent scattering sites [30,31]. Electron oscillations also produce losses through resistive loss and direct decay of electrons to phonons. These losses generate heat and are in the form of absorption of light. Localized heating from nanoparticles has been used in applications involving thermal ablation of cells and heating [32–35], selective fabrication methods [36–39], and of a medium through absorbed light [40–44].

Controlling the size, shape, composition, and medium surrounding the nanoparticles allows tunability of the type of decay (scattering and absorption) as well as of the spectral region of light that is converted to a plasmon. It has been shown that increases in the carrier density shift plasmon resonance to higher energies [45,46]. While metals cannot exhibit changes in their carrier density, shape variations allow isolation and concentration of electron oscillation to affect the resonance energy. Metal nanoparticles typically convert UV and visible light, but can also convert IR light for special shapes such as rods. Semiconductor and metal oxides convert near to mid-IR light and are tuned by changing particle size and shape in addition to chemical doping. For example, changing the oxygen depletion in tungsten-oxide nanocrystals alters the carrier density and thus the location of the resonance [47]. Linear materials, such as metals, exhibit an induced polarizability when interacting with an external electric field. For particles where dipole modeling can approximate the optical behavior, polarization of a material in an electric field can be expressed by

$$\boldsymbol{P} = \alpha \boldsymbol{E}, \tag{1}$$

where $\boldsymbol{P}$ is the induced polarization, $\boldsymbol{E}$ is the external electric field, and α is the particle polarizability. Several models exist to describe particle polarizability for various circumstances. A brief outline of salient polarizability models for nanoparticles is given below.

For nanoparticles much smaller than the incident wavelength of light, the wave can be assumed to be uniform. In this case, the well-known Claussius–Mosotti (CM) polarizability can be applied. This form of polarizability is given by

$$\alpha_{\mathrm{CM}} = R^3 \frac{\epsilon_m - 1}{\epsilon_m + 2}, \tag{2}$$

where R is the particle radius and ϵ_m is the ratio of refractive indices inside to outside the particle. From Eq. (2), it is observed that plasmon resonance occurs when the real component of ϵ_m is equal to -2. This can only occur in materials with a high free carrier density.

Table 1. Selected Polarizability Models for Various Nanoparticle Formulations

Polarizability Model	Nanoparticle Morphology and Composition	References
CM	Small metal spheres (<25 nm diameter); semiconducting nanocrystals; metal oxide nanocrystal	[41,52]
MLWA [53]	Large metal spheres (25–150 nm diameter)	
Mie-based [28,48]	Metal spheres (diameter up to 500 nm)	[50,51,54]
Core–shell [55]	Core–shell (composition variable)	[56–59]
Shape-corrected [60]	Elongated (or squished) metal shapes	[41,61,62]
Toroidal [49]	Metal ring or toroid shapes	[31,63–66]

The CM polarizability is not suited for all nanoparticle types. Additions to the polarizability model are required for particles that have larger sizes, nonspherical shapes, or are composed of multiple materials. For larger particles, scattering and electron dephasing cause redshifts in the primary plasmon peak. This can be accounted for by including dynamic effects from the nonuniform electric field across the nanoparticle using the modified long wavelength approximation (MLWA). An exact dipole polarizability has been developed using the Mie coefficients, but is only applicable under the same assumptions that Mie theory is built on [48]. Particles with asymmetry, such as rods or squished spheres, can be modeled using shape-adjusted polarizability models. Additional polarizability models have been created to account for core–shells, toroidal structures, [49] and quadrupole terms for larger particles [50,51]. Table 1 displays various nanoparticle types with appropriate polarizability models for each.

To determine how intrinsic particle properties effect plasmon resonance, an expression for the particular material's dielectric function must be known. It has been shown that the Drude model provides an appropriate approximation to describe plasmonic materials dielectric function, including doped semiconductors, in the visible to near IR region where plasmonic behavior is observed [45,46,67]. The dielectric function is then used in Eq. (2) to determine the polarizability of a nanoparticle. It is noted that the dielectric function is the same for any particular material type, excluding effects of nonlocality for nanostructures with dimensions less than the mean free path, which is outside the scope of this review [68–70]. As a result, optical properties for a nanoparticle are dictated more by the polarizability than by the dielectric function.

2.2. Quadrupole Modeling

Larger nanoparticles, with respect to incident wavelength of light, can support higher order electric modes, such as the quadrupole mode. This is a result a spatiotemporal perturbation of the electric field across the particle, allowing electrons to flow to physically different locations on the nanoparticle. To account for this effect, a quadrupole polarizability must be used to describe the behavior of this mode. The quadrupole polarizability expression has received far less attention than the dipole expressions given above due to the lesser appearance of higher order electric modes in viable applications. However, this is an important consideration when nanoparticle sizes begin to reach approximately 150 nm in diameter, depending on the composition of the nanoparticle. For example, Ag nanoparticles have the quadrupole mode appear at smaller radii as compared to Au nanoparticles. When the nanoparticles are sized near this lower limit for quadrupole excitation, a quasi-static approximation (analogous to the CM dipole approximation) can be done. This approach gives the following expression for the quadrupole polarizability:

$$\alpha_q = R^5 \frac{\epsilon_m - 1}{\epsilon_m + 3/2}, \tag{3}$$

where R and ϵ_m are defined as before [71]. The primary differences between α_{CM} and α_q is the order of the exponent of the particle radius [due to the expressions of the electric field and Eq. (1)] and the denominator changing from a 2 to a 3/2. The smaller value in the denominator signifies that the quadrupole mode appears at wavelengths that are blueshifted compared to the dipole mode.

Similar to the dipole case, there have been limited expansions to the quadrupole polarizability. Namely, work has been done to express larger nanoparticles with a quadrupole term using Mie coefficients [51,72]. However, work involving higher order electric modes has been primarily limited to spheres. This is because there is a vast variability in the possible shapes for larger nanostructures and many higher order effects, such as phase shift and depolarization, are difficult to account for. As a result, numerical and other approximation methods, such as the discrete dipole approximation (DDA) [73–76], have been used to determine higher order optical properties from arbitrarily shaped and sized nanoparticles.

2.3. Scattering

Scattering is process by which the energy of incident light is conserved, but its propagation direction is altered. For particles much smaller than the incident wavelength of light, the individual nanoparticles can be treated as a point dipole with the dipole oscillation in the direction of light polarization. In this way, the nanoparticles act as mini antennae to re-radiate light that was converted to a plasmon oscillation. Since the nanoparticles oscillate as dipoles, the re-radiation of light follows the pattern of dipole radiation. The scattering cross section can be computed using

$$\sigma_{\mathrm{sca,dipole}} = \frac{8}{3}\pi k^4 |\alpha|^2, \tag{4}$$

where k is the wavenumber in the media and α is the dipole polarizability of the particle [45,55].

As nanoparticle sizes increase relative to the wavelength of light, electric quadrupole modes can be excited. The scattering cross section is more complicated to calculate than that of a dipole in Eq. (4). The expression for the quadrupole scattering cross section for the quasi-static approximation is given as

$$\sigma_{\mathrm{sca,quad}} = \frac{8}{3}\pi k^4 \left(\frac{k^4}{240} |\alpha_q|^2 + \frac{k^4}{900} |\epsilon_m - 1|^2 \right), \tag{5}$$

where the terms are as defined previously [71]. Scattering from a quadrupole mode follows the radiation pattern of an oscillating quadrupole. The scattering profile for dipole and quadrupole modes are given in Fig. 2. The amplitude of the scattering intensity for the dipole and quadrupole modes scale with $\sin^2(\theta)$ and $\sin^2(\theta)\cos^2(\theta)$, respectively, where θ is the angle away from the direction of light polarization. From the figure, it is apparent that forward scattering (i.e., no change in the light prorogation direction) can occur for dipoles, but not for quadrupoles. For nanoparticles in a colloidal suspension with random distributions, the scattering profile (electric field distribution) does not significantly affect coupling between particles. However, when nanoparticles are arranged in a solid-state lattice, careful attention must be placed on the arrangement of the nanoparticles to ensure appropriate coupling from the electric field generated by neighboring particles.

2.4. Absorption

Absorption is a nonreversible process by which some (or most) of the incident light is converted to heat. The physical mechanism can be a plasmon that directly decays to a phonon or through the process of ohmic losses. Since the electrons are oscillating inside the nanoparticles, typical resistive losses are still present and contribute to heat generation in the particle. The absorption cross section for an induced oscillating dipole is given as

$$\sigma_{\text{Abs}} = 4\pi k \,\text{Im}\{\alpha\}, \tag{6}$$

where k and α are as defined previously [45].

Absorption dominates for particles much smaller than the incident wavelength of light. This holds true for both dipole and quadrupole modes. As nanoparticles increase in size, more of the plasmon decays into scattering, and the relative contributions begin to even out. As the nanoparticles increase more in size, scattering becomes dominant and absorption becomes minimized. One reason for this is that the time scale for scattering decay decreases as the nanoparticle size increases, giving a larger probability that the plasmon will decay into a photon as opposed to a phonon. Additionally, contributions to scattering and absorption are independent of the excited mode. For example, when nanoparticles are large enough to support quadrupole excitation, absorption dominates in the quadrupole mode, while scattering dominates in the dipole mode. When deciding on a particular application that involves scattering or absorption of light, these effects must be optimized for commercial viability of the research.

2.5. Emission

Nanoparticles can give off electromagnetic radiation via thermal (blackbody), photoluminescent, or phosphorescent emission. Plasmon resonance of nanomaterials can also be employed in the terahertz-emission range to strongly enhance the emission rate of quantum systems (e.g., nano-antennas in the ∼5–15 μm wavelength range [77]), but these applications will not be covered in detail in this review since these do not include mechanisms in optical range.

For thermal, photoluminescent, or phosphorescent emission to be significant, the nanoparticles must be at a higher energy state than their ground state and/or their immediate surroundings (thermally and/or electronically). In the case of thermal emission, this means that the nanoparticles should be at a significantly higher temperature relative to the surrounding environment. In most, but not all, applications, thermal emission results from the absorption properties of the nanoparticles and primarily

Figure 2

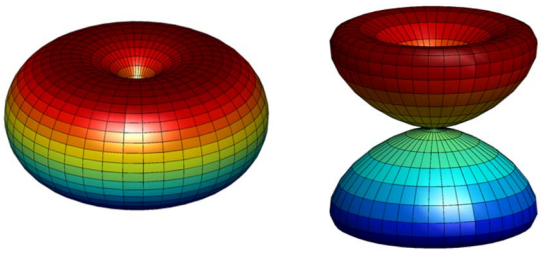

(a) (b)

Representation of (a) dipole and (b) quadrupole scattering with light polarized along the z (vertical) axis.

consists of diffuse, long wavelength (>3 μm) emission, which is particularly true for the temperatures in the applications discussed below. In this category, it may be possible to design nanoparticles that have minimal (or even maximal) long wavelength emissivity through geometry, shape, and material nanoparticle design choices.

Photoluminescence and phosphorescence occur after light has been absorbed, temporarily exciting the nanoparticle's electronic states. (Note: While other means of photoluminescence and phosphorescence excitation have potential, within the scope of this review we will focus on photoexcitation.) The absolute quantum yield can be calculated using an integrating sphere and measuring against a well-known, standard sample (typically a fluorescent dye such as Rhodamine). The following equation, which matches with fluorescence quantum yield, can be used:

$$\varphi_{\mathrm{NP}} = \varphi_{\mathrm{std}}\left(\frac{\mathrm{Grad}_{\mathrm{NP}}}{\mathrm{Grad}_{\mathrm{std}}}\right)\left(\frac{n_{\mathrm{NP}}^2}{n_{\mathrm{std}}^2}\right). \tag{7}$$

The subscripts "NP" and "std" represent the nanoparticle and the well-known standard sample, respectively, and φ is the photoluminescence quantum yield. The first ratio, denoted by "Grad" in the equation, is the gradient of the plot of total hemispherical integrated intensity versus absorbance. The n values in the last ratio term represent the refractive index of the medium, since different fluids/films or different temperatures could alter the yield.

Depending on the quantum yield of the process, a portion of this energy can then be released quickly (e.g., by photoluminescence, of the order of picoseconds or nanoseconds) or at a later time (e.g., by phosphorescence, of the order of seconds or even hours) in the form of radiative emission. Since this type of emission is generally confined to a narrow window (typically in the visible spectrum), it is possible to "shift" incident light from its original spectrum to a more desirable spectrum for the application. Since photoluminescence and phosphorescence are (generally) diffuse, it is also possible to change the direction of propagation from the original incident light.

3. SYNTHESIS

There are two primary classifications for synthesizing nanoparticles and nanostructures. The first approach, bottom-up, starts with precursor materials to build individual nanoparticles or nanostructures through a variety of reactions. The second approach, top-down, utilizes a host material/target through which a large amount of energy is imparted (in a variety of forms) to release nanoparticles from the target which are subsequently collected as nanoparticles at a different site. A vast number of review articles and detailed methods exist for the synthesis of nanoparticles; highlighted here is a selection of techniques and review articles that are commonly used.

The most common approach to the synthesis of nanoparticles is the bottom-up approach, and the development of bottom-up approaches is most widespread in the synthesis of gold nanoparticles. Zhao *et al.* has provided a review of recent developments in the synthesis of gold particles [78] that outlines that the most prevalent methods are still chemical reduction/precipitation methods. In particular, one of the most common approaches is the Turkevich method, in which nanoparticles are prepared by the reduction of $HAuCl_4$. In this method, $HAuCl_4$ solution is boiled, and then trisodium citrate dihydrate is added and vigorously stirred, resulting in 20 nm particles [79]. Over the years many approaches have modified the chemical reduction method to achieve particles of different sizes, shapes, and materials [78,80–82]. In addition to the chemical reduction approach, other bottom-up approaches are microemulsion (use

of microemulsion solutions for controlled size growth), thermal decomposition (chemical decomposition at high temperatures), hydrothermal synthesis (high temperature and pressure reaction), sol-gel (polymerization), sonochemical (application of ultrasonic radiation), and radiolysis (gamma irradiation) [78–83].

Top-down approaches are most commonly utilized in approaches in which a substrate is being coated and only small amounts are required, although approaches do exist for large volume production. Arguably the simplest method, in principle, is via ball milling. In this approach, bulk powder or material is put into a ball mill or grinder and is ground down to subsequently finer and finer powders until nanoparticles are formed. This approach is quite simple, but it requires extremely long times and can result in significant changes to crystal structure due to the high amount of energy imparted during the process [83,84]. Another approach is laser ablation, in which high-energy lasers irradiate a target solid. This evaporates a small portion of the target, which can then be rapidly condensed to form a nanoparticle on a surface or directly within a liquid [85,86]. Other approaches, such as arc discharge and chemical vapor deposition, are widely used and can produce well-defined size distributions, albeit in small quantities [83,86]. In addition to the review papers cited in this section, papers citing specific particle types and properties all include descriptions of the various synthesis techniques to generate the referenced particles.

There are four primary factors that affect the cost of the fabricated nanoparticles and structures: material cost, equipment cost, labor cost, and overhead. As a rule of thumb, the "cost floor" of any single material particle is the spot price of the material. Utilizing one of the most common nanoparticles, gold spheres, a range of prices for a 10 nm sphere can be obtained from $40,000–$80,000/gram [87–89]. As of this writing, the spot price of gold was $43/gram [90]; the cost of nanoparticles is roughly 1000 times more than this. As seen, the cost of nanoparticles still greatly exceeds the cost of the base material itself. As noted, one of the advantages of using nanoparticles for their optical benefits is the extremely small amount of material needed, which results in minimal impact to system cost.

4. NANO-ENGINEERED OPTICAL PROPERTIES

Plasmon absorption and scattering depend on a number of factors—e.g., size, shape, composition, surrounding media, and proximity to one another. In general, increasing the size of a nanoparticle redshifts the peak plasmon wavelength.

4.1. Material Effects

Plasmon resonance is affected by composition changes through spectral shifting and broadening. The physical mechanism behind this plasmon behavior is free carrier density and plasmon decay through losses in the material. Free carrier density increases typically blueshift the plasmon peak wavelength to shorter wavelengths. Choosing either metals with high carrier density, which generally resonate in the UV to visible range, or semiconductors with variable carrier density allows for custom-designed resonance over a wide range of values from 300 to over 3000 nm.

Tunability of plasmon resonance for a single nanoparticle type is only possible for nonmetals. Metallic nanoparticles have a set carrier density, and changes cannot be made without charging the nanoparticle. However, metal oxides and semiconducting nanostructures can have a variable plasmon resonance through changes in composition from doping. Metal oxides have a variable carrier concentration through changes in oxide concentration. For example, copper chalcogenide nanocrystals possess a variable free carrier concentration through adjustments to the copper stoichiometry [91]. Copper deficiency changes the carrier concentration and, thus, the

Table 2. Nanoparticles and Their Selectivity in Absorbing Light

Nanoparticle Type	Size Range	Absorption Range	Tuning Parameter	References
Metal sphere	10–300 nm diameter	300–1000 nm	Size	[48,59,68,94]
Metal rod	5–30 nm diameter, 50–200 nm length	300–1800 nm	Aspect ratio	[59,62,95–98]
Metal oxide rod	20–50 nm diameter, hundreds on nm length	780–2500 nm	Carrier density (metal or oxygen content)	[99–101]
Indium tin oxide	5–30 nm diameter	1600–2500 nm	Tin doping	[62,93,102]
Antimony tin oxide	5–30 nm diameter	~2200 nm	Oxygen deficiency	[62,103]
Zinc oxide	5–30 nm diameter	2000–2500 nm	UV-light; metal doping	[45,46]
Hexaboride crystals	10–150 nm diameter	700–1500 nm	Stoichiometry	[104]
Chalcogenides	10–50 nm diameter	800–1600 nm	Copper content	[91,105,106]

dielectric function of the nanocrystals, causing a shift in plasmon resonance [45,46]. Similarly, indium–tin-oxide (ITO) nanocrystals and tungsten-oxide (WO) nanocrystals have variable concentrations through tin and oxygen doping in the nanocrystals [45,46,92,93]. A variety of nanocrystal types provide varying degrees of plasmon resonance tuning. Ultimately, the choice of nanoparticle depends on specific wavelength ranges desired for light filtration in addition to the potential of the nanocrystal to be optically and colloidally stable in the solution [62]. Table 2 summarizes various nanoparticle types, the absorption bands, and tunability parameters for selective filtration. Figure 3 illustrates absorption bands of various different types of nanoparticles. Table 2 is meant to be an overview of potential materials, and it should be recognized that a large number of materials and material combinations are possible, including combinations of plasmonic metals with other plasmonic metals [107], dielectrics, and with semiconductors [108].

4.2. Media Effects

Surrounding media causes shifts and amplitude changes in plasmonic behavior. Increasing the refractive index around a particle effectively increases the number of molecules capable of producing induced molecular dipoles in the media itself in response to the electron oscillation. This acts to dampen the coulombic restoring force and decreases the energy of oscillation (e.g., causing a redshift) [54]. In addition, incident wavelengths for particles in an increased refractive index environment experience contraction. The smaller wavelength exaggerates the particle-size to vacuum-wavelength ratio, responsible for effects not taken into account using the CM polarizability. This reduces the radius limits for the polarizabilities discussed in Table 2. This concept is illustrated in Fig. 4. Figure 4 shows how the plasmon resonance of a gold nanoparticle with 100 nm diameter changes with increasing

Figure 3

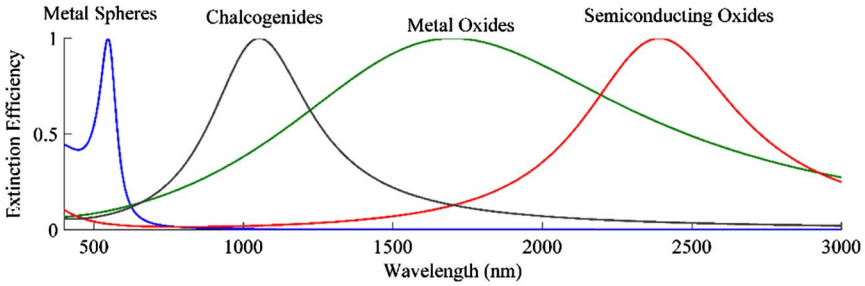

Representative absorption spectra calculated for various types of nanoparticles, as labeled in the graph.

refractive index. As refractive index goes from vacuum to water to silica, the resonance redshifts and increases in intensity.

4.3. Morphological Effects

Changing the shape of particles modifies the oscillation of surface electrons, causing shifts in the resonant energy. Morphology changes can alter the way in which electrons can oscillate on the surface, causing surface interactions within the particle [65,71,109–111], splitting or hybridization of plasmon modes [112–114], and nonlocal effects [68,115]. Sharp points or regions of high curvature allow strong confinement of electric fields [110]. These effects cause shifting and amplitude variations as well as near-field enhancements for applications where close proximity to the particle can have strong effects.

The three most prominent and easily modeled shape modifications that are used to control plasmon oscillation for colloidal nanostructures are (i) scaling, (ii) squishing or elongating a particle, and (iii) core–shell morphologies. For example, a sphere can be squished into a disk or even elongated into a rod. Each of these effects can be simulated using an extension to the CM polarizability by modification of the equation using a shape parameter [61,71,116–118]. Scaling nanoparticles by size tends to increase scattering and redshift the plasmon resonance. Resonance redshifting is illustrated in Fig. 5 with gold nanoparticles simulated at different diameters. An increase in one dimension of a nanostructure causes asymmetry in the particle. This effect enables two plasmon modes to be supported on the particle, one for each axis of elongation. Typically, light polarization can affect plasmon modes [119,120]. However,

Figure 4

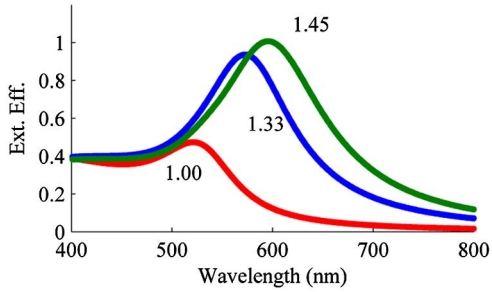

Gold nanoparticle with diameter of 100 nm in media with refractive indices of 1.00, 1.33, and 1.45, as labeled in the figure.

Figure 5

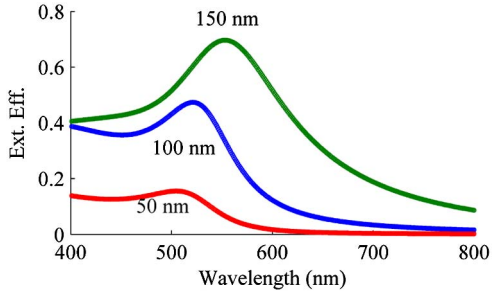

Illustrating size effects for a gold nanoparticle with diameter increasing from 50 to 100 to 150 nm.

nonpolarized light and the random orientation of colloidal nanoparticles allow both plasmon modes to be excited simultaneously. The primary plasmon peak is observed to be a result of the long axis, and can shift as aspect ratio is adjusted. As a general rule, as the aspect ratio of a structure increases, the plasmon resonance redshifts to longer wavelengths [59,121,122]. The short axis plasmon peak remains relatively unchanged for variable aspect ratio. This concept for gold rods is illustrated in Fig. 6. In the figure, a 10 nm short diameter nanorod with varying lengths is shown to see how the plasmon peak redshifts with increasing aspect ratio.

Core–shell morphologies or shapes with surfaces near each other also possess unique optical properties from surface–surface interactions in a single nanostructure. Core–shell particles are illustrated in Fig. 7 for a silica-core–Au-shell construct with a 100 nm diameter silica core and decreasing Au shell thicknesses. Core–shell morphologies allow certain dimensions to be small compared to the overall size of the particle. Particles with a plasmonic core and dielectric shell are not significantly different than uncoated plasmonic nanoparticles, with the exception of a slightly modified surrounding refractive index.

In addition to the three classes of morphologies above, a variety of combinations and novel structures have been successfully synthesized, but it should be noted that their optical properties fall within the considerations of the effects outlined above for sphere, rod, and core–shell morphologies. Self-interacting structures can be achieved with triagonal prisms, with further tuning from snipping corners [71], decahedral particles that demonstrate two plasmon peaks and bicolor behavior [123],

Figure 6

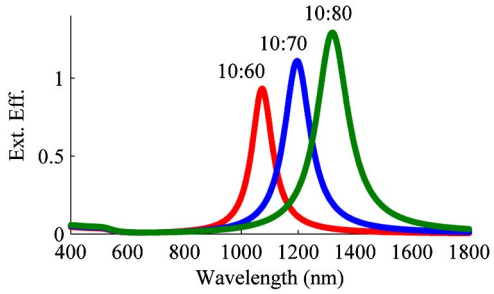

Simulated spectra of nanorods with short diameter of 10 nm and length of 60, 70, and 80 nm.

Figure 7

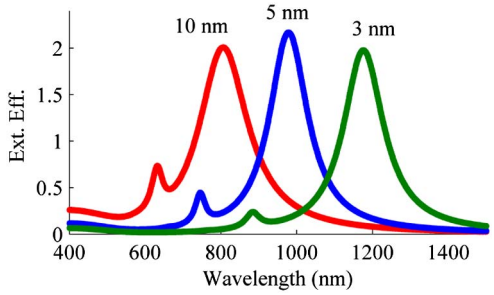

Spectra for core–shell particles with a 100 nm diameter silica core and shrinking gold shell size of 10, 5, and 3 nm.

nanocups [124,125], nanomatryoshkas (plasmonic core, silica layer, plasmonic shell), which show enhanced fluorescence [126], nanocages (redshifting of plasmon peak) [127], multishell particles [107], nanorings [31,66], and silver-coated gold nanorods, which exhibit blueshifting of the longitudinal plasmon peak [128], among other combined plasmonic materials in sphere and rod geometry [27].

4.4. Particle–Particle Interactions

Nanoparticles in proximity to each other can interact and modify the resonance location. This effect can be seen in both suspension and solid-state arrangements. This effect is dependent on the incident polarization of light, since the induced plasmon oscillation will oscillate in the direction of the incident electric field from the light. The induced electron oscillation is an effective oscillating dipole that produces near-, intermediate-, and far-field effects depending on the size of the particle. Smaller particles are predominately absorption, leading to mainly near-field effects. Larger particles predominately scatter light, leading to far-field effects.

Suspended particles are typically of low enough concentrations that direct interactions from neighboring nanoparticles can be ignored [129]. However, nanoparticles can agglomerate into larger particles, causing an effective increase in size. This is caused by settling over time and chemical interactions between surfactants. This results in a redshifted resonance and an increase in scattering. Additionally, particles can be designed such that they are in close proximity or attached while in solution. Primarily, this has been utilized for coupling gold nanoparticles to quantum dots for enhanced photoluminescence [130] and for tunable upconversion [131]. Another approach demonstrated in suspensions has been proposed as a means to dynamically control radiative transport [132–134], but it is fairly limited by geometry to small spectral shifts.

Nanoparticles in close proximity have been shown to have strong localized electric fields and have been called gap plasmons. Illuminated nanoparticles with a strong gap plasmon can attract single molecules between them, which alters the electric field for single molecule sensing applications [135]. This same effect has been suggested as a method to self-organize nanoparticles into chains or arrays [136]. Assembly of single nanoparticles into controlled agglomerates allows tunability for selective scattering and absorption properties [137,138].

Creation of thin films of nanoparticles can result in controlled spacing and arrangement into arrays, which leads to nanoparticle interaction and causes plasmon shifting and amplitude variations. This effect has been studied for a multitude of nanoparticle arrays with a particular emphasis on gold nanoparticles with controlled spacing [139–141]. These results indicate that redshifting occurs as the particle spacing is decreased. Further work has investigated a similar effect but for ellipsoids, rods, and cylinders where the impact of spacing and aspect ratio is studied for gold [142] and gold/silver [143]. For this geometry, decreases in spacing result in blueshifting.

5. NANOPARTICLE-BASED DEVICES AND APPLICATIONS

A single nanoparticle cannot absorb a significant amount of light for real-world applications. However, a collection of nanoparticles (at very low volume fractions, typically $\ll 0.1\%$) embedded in a medium can absorb 100% of the light in a particular energy band [62]. Light filtration can occur for nanoparticles in a liquid suspension or for a planar arrangement of nanostructures in a two-dimensional matrix. We discuss relevant and recent applications of such approaches below, with a specific focus on applications in which nanoparticles are used to absorb/scatter a limited spectrum of incident radiation.

5.1. Applications in Liquids

Nanoparticles suspended in liquids can modify the optical properties of the entire embedding fluid. This has been accomplished at surprisingly low volume fraction, of the order of 10^{-6} to 10^{-8}. This allows modification of fluid optics while using a minimal amount of nanoparticles, helping to keep associated costs down. Additionally, the ability to control the volume fraction allows for close coupling between the fluid's and the nanoparticles' spectral absorption properties. For example, most liquids are highly transparent in visible wavelengths with strong absorption bands distributed throughout the infrared (IR) [144]. Using a combination of nanoparticles with absorption peaks that do not overlap, broad absorption of the base fluid can be achieved. Additionally, this can be done for thin to thick liquid paths by varying the volume fraction.

5.1a. Selective Absorption

Applications in Solar Energy Systems. Spectral light filtration in liquids using nanoparticles has primarily been proposed in liquids for one purpose, photothermal energy conversion in solar thermal collectors. The basic options for this are shown in Fig. 8. In the case of solar thermal energy systems, the primary application has been the selective filtration of solar energy in hybrid photovoltaic/thermal (PV/T) collectors. The concept of fluid-based filtration has been around since the 1980s [2], and has seen a recent resurgence where a pure liquid acts as the filter [13,145–147]. All of these papers note the limited ability of the fluid to absorb key wavelength bands due to the inherently fixed absorption properties of the fluid. A recent paper attempted to address this limitation with the addition of copper sulfate salts to enhance the UV–visible absorption while creating no enhancement in the IR [148]. The first known proposal for achieving this with nanoparticles assessed the performance of an ideal collector [149], which was shortly thereafter followed by an analysis of metal plasmonic nanoparticles for optical efficiency in different cell materials [150]. Further work looked to assess the feasibility from a cost perspective of such nanoparticles based on early research-grade prices into core–shell particles [151]. This work revealed cost challenges as well as difficulty in synthesis routines that would result in high-UV-Vis absorption using core–shell particles [151]. These initial studies revealed that success in PV/T systems would need to go beyond classic metal sphere and core–shell type nanoparticles, since these have difficulty in effectively absorbing IR wavelengths without degrading transmission in the visible. It seems this challenge has

Figure 8

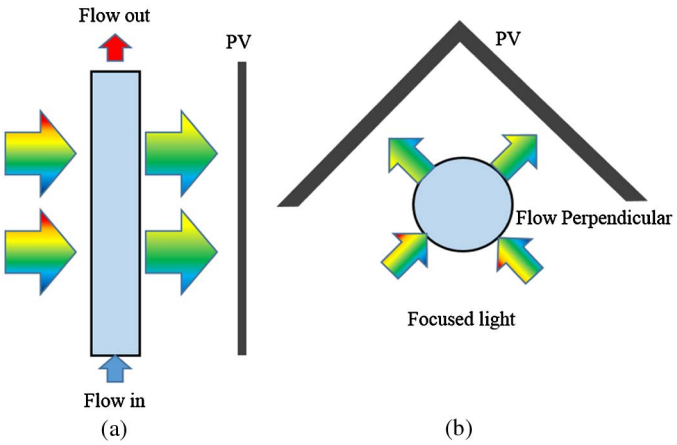

Schematic diagram of nanoparticle filters in CPV/T for (a) flat low concentration of one sun system and (b) concentrating system with an annulus design.

now been overcome by considering nanorod geometry and semiconducting nanoparticles that exhibit plasmon resonance further into the IR [62]. All of these particle choices, however, must be balanced with secondary plasmon peaks—which, in the case of metals, are often in the visible region but are significantly weaker than the primary peak or the high UV scattering of semiconducting nanoparticles. Additional recent studies have numerically investigated combinations of silver prisms and carbon nanotubes (nonselective) [152]. Benchtop nonflowing tests have considered polypyrrole nanoparticles (nonselective) [153]. Researchers have also done considerable numerical modeling and optical property testing of silica (selective, but predominantly UV–vis scattering) nanoparticles [154], optimization of filter design for differing cell materials with experimentally measured optical properties for gold–silica core–shell particles, silica-coated gold nanorods, and ITO semiconducting nanocrystals [98]. Further numerical studies have investigated the impact of temperature-dependent bandgaps on optimal filtering design [155]. All of these studies indicate that nanoparticle-based filtering for CPV/T operations is a nascent area that still has a lot of room for improvement and for designing suitable combinations of nanoparticles, base liquid, PV cell selection, and system architecture to optimize both the electrical and the thermal energy output.

5.1b. Selective Scattering

The most widespread use of nanoparticles outside of research laboratories has been in consumer products, particularly the use of metal oxides in sunscreens [156]. These particles are extremely efficient at scattering damaging UVA and UVB radiation while easily being integrated into the base material. Titanium dioxide is more effective in the UVB region, while zinc oxide is more effective for the UVA range [157]. Sunscreens consisting of both of these nanoparticles are available, but a significant amount of research is focused on the long-term safety of these sunscreens [157]. The optical properties of titanium oxide are particularly useful in sunscreen and cosmetics as a white pigment, and it is used as well in paints [158].

Another use of scattering nanoparticles is for reflection back into an application. Mendes *et al.* proposed a backreflector of colloidal suspension nanoparticles for enhanced efficiency in silicon solar cells [159]. In this application, shown in Fig. 9, aqueous suspensions of 100–200 nm gold nanospheres with high scattering cross sections are placed between the silicon cell and the normal backreflector to improve reflection of the longer solar wavelengths. Up to 60% reflectance was achieved at wavelengths >850 nm for the largest gold nanoparticles [159].

Figure 9

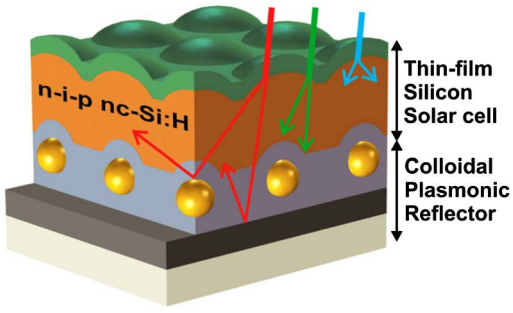

Schematic of a colloidal plasmonic backreflector for enhancement of silicon cell light trapping, developed by Mendes *et al.* [159]. Reprinted from Mendes *et al.*, Nanotechnology, **26**, 135202 (2015) [159].

5.1c. Selective Emission

As mentioned above, nanoparticle emission can result from optically derived thermal and electronic excitation of nanoparticles. As nanoparticles absorb light they will, in general, experience both electronic and thermal excitation, but (in most cases) will come to equilibrium with the local surrounding liquid relatively rapidly. Liquid applications of this type have a major advantage in that they can be pumped in and out of a system to achieve any desired temporal variation in their emission. As compared to selective absorption and scattering, this category of optical selectivity may be less developed.

One field of research where nanoparticle selective emission is making a big impact is in biomedical applications. In these applications, the nanoparticles are surrounded by fluids and often dynamically flow during their use. A number of research papers have indicated that nanoparticles that exhibit photoluminescence themselves or carry photoluminescent (or fluorescent) materials, are very promising for biolabeling, detection, sensing, and imaging. To achieve these aims, the nanoparticle could also be coated with a targeting material that would enable it to selectively attach to certain cell types. For maximum signal to noise, the photoluminescence signal would emanate from the nanoparticle only once it has found the specific target cell(s). In a study by Hua *et al.* [160], SiO_2 nanoparticles were coated with CdTe quantum dots (which have bright red photoluminescence at 600–680 nm) to quantitatively detect MCF-7 (breast cancer) cells. Their study found that, by using photoluminescence, these materials were indeed capable of attaching to the MCF-7 cells and could detect as little as 85 cells per ml [160]. Sun *et al.* [161] suspended single-layer, small (>100 nm length) sheets of graphene oxide in water. These materials were found to have good potential for visible and near-infrared (NIR) imaging of live cells using photoluminescence—a schematic of their approach is shown in Fig. 10 [161].

In a study by Welsher *et al.* [162], single-walled carbon nanotubes (SWCNTs) were used as tags for probing cell surface receptors and for cell imaging. In this research, the SWCNTs were coated with antibodies that were able to recognize cancer (breast and lymphoma) cells to detect these types of cells in the body. Figure 11 shows the photoluminescence, a microscopy image, and schematics of these types of nanoparticles.

Figure 10

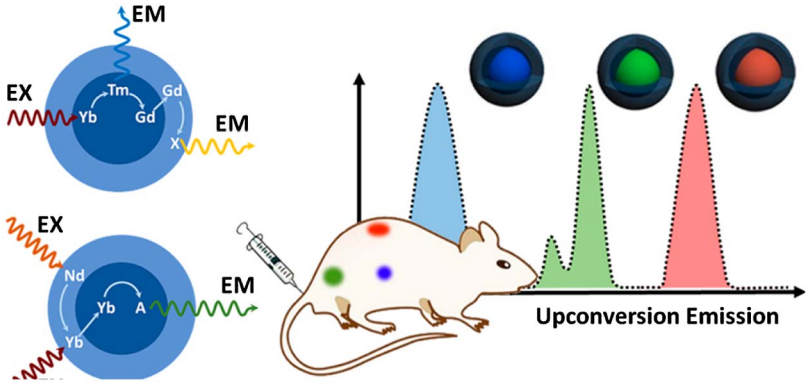

Graphene-nanosheet-based imaging scheme by Sun *et al.* [161]. Reprinted with permission from Sun *et al.*, Acc. Chem. Res. **47**, 1001–1009 (2014) [161]. Copyright (2014) American Chemical Society.

Quantum dots can also be used as emitter for biomedical applications. In a communication by Dubach *et al.* [163], quantum dots were coated by two concentric polymer layers to achieve an ~100 nm nanosphere with a fluorescent peak at 650 nm under UV excitation. The outer polymer coating of these particles was reported to be biocompatible while the inner layer is an ion-selective polymer, which controlled the fluorescent intensity based on the surrounding ion concentration [163]. Thus, these nanoparticles, shown in Fig. 12, can be used as optical sensors to determine the concentration of salt ions in the local environment.

Figure 11

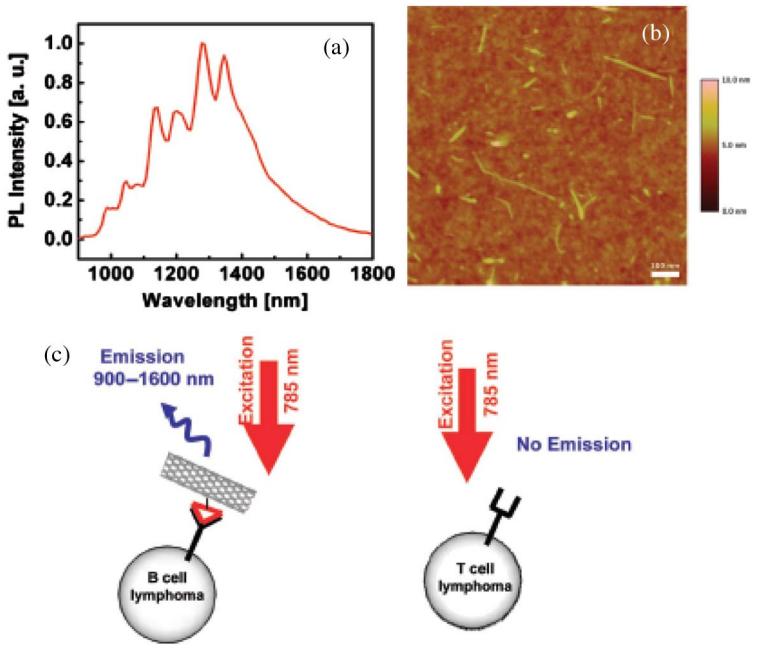

(a) NIR photoluminescence spectrum of a SWCNT conjugate, showing typical SWNT emission peaks. (b) Atomic force microscopy image of the nanoparticles (average diameter ~1.6 nm, average length ~83 nm) (c) Schematic of photoluminescence (PL) detection of selective B-cell versus T-cell lymphoma [162]. Reprinted with permission from Welsher *et al.*, Nano Lett. **8**, 586–590 (2008) [162]. Copyright (2008) American Chemical Society.

Figure 12

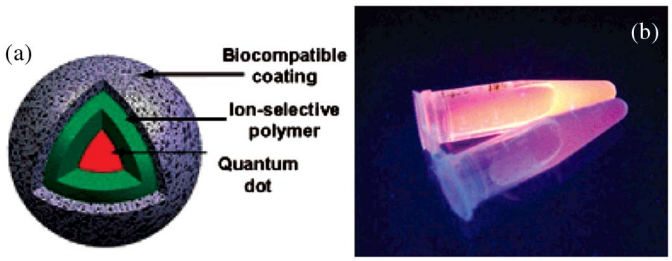

(a) Schematic of the polymer-coated quantum dot and (b) photograph of a liquid suspension of the nanoparticles developed by Dubach *et al.* [163]. Reprinted with permission from Dubach *et al.*, J. Am. Chem. Soc. **129**, 8418–8419 (2007) [162]. Copyright (2007) American Chemical Society.

Masuda *et al.* [164] found that the photoluminescent spectra (UV–visible) of ZnO crystals can be controlled by changing the conditions in an aqueous suspension during deposition on a silicon wafer. Depending on the conditions during synthesis, various morphologies of ZnO were found (hexagonal cylinders, ellipses, and multi-needles). These very different morphologies led to strong photoluminescence between 350–600 nm [164]. Xu *et al.* [165] also looked at a wide variety of morphologies, but of more exotic materials—YVO_4 nanoparticles doped with Dy, Er, Eu, and Sm—for their luminescent properties. In the study by Xu *et al.*, particle diameters ranged from 15 nm to 1 μm and morphologies included spheres, disks, rods, plates, flowers, and even doughnuts. Using a UV excitation source (254 nm), it was found that these materials have strong red, orange–red, green–yellow, and green emission peaks with quantum efficiencies in the range of 50%–70% [165].

While the vast majority of spectral emission in fluid-based systems is focused on control of luminescence, there is the potential for spectral control of thermal emission. The primary challenge with enhancing or controlling thermal emission in fluids is that most of the thermal properties in the IR are dictated by the base fluid. There still exists a desire to potentially use thermal emission from nanoparticles that can be tuned to emit near the spectral peak of the blackbody spectrum. One numerical study focused on the role of radiative cooling of nanoparticles close to a surface for both plasmonic (Au) and polar (SiC) materials [166]. The polar materials support a surface phonon polariton in the IR, versus the plasmon mode in the visible. The aforementioned study focused primarily on the thermal relaxation dynamics and not on any potential system. Two proposed systems that take advantage of nanoparticle thermal emission have been described for radiative sky cooling systems [167] and in variable emittance radiators for spacecraft [168]. Both studies are limited by assuming an ideal fluid that does not interact with the nanoparticles. The latter study achieves controllable emittance through reversible size changes that result in changes to the overall volume fraction, as seen in Fig. 13. This is another area for further exciting developments, as the further understanding and design of new fluids and materials could lead to exciting heat rejection technologies.

5.2. Applications in Thin Films

Nanoparticles situated on top of a material can modify how light is directed into and through the interface. We focus here on recent applications or critical reviews where

Figure 13

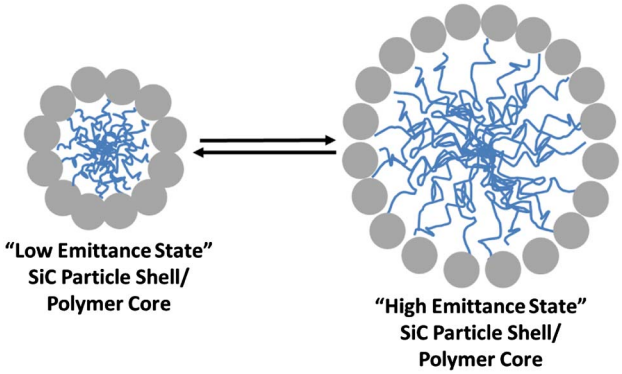

Schematic of proposed size-induced changes in emittance. Shell particles are made of SiC material with high emissivity in the IR and a reversible swelling core polymer.

the nanoparticles are independent objects, not deposited and sintered together, as is done in many applications. Our goal is not an exhaustive review of each application, but highlighting key works.

5.2a. Selective Absorption

Applications in Windows. One specific application of thin-film-based nanoparticles for spectrally selective filtering is for use on windows as a means to create alternative coatings capable of blocking NIR solar energy into buildings to limit solar-driven cooling. Early applications focused on "static applications" in which the nanoparticles are applied in a thin coat to the window. Promising candidates are rare-earth hexaborides [104], where the rare-earth element is gadolinium, neodymium, praseodymium, cesium, or lanthanum. These particles have an absorption peak centered around 1000 nm, where the strength of the peak is directly tied to the lattice constant of the material. From this reference, it appears that lanthanum hexaboride is one of the most promising candidates of the hexaborides for solar NIR absorbing materials [104]. To our knowledge, the use of nanorods or core–shell nanoparticles has not yet been explored in window applications for blocking NIR radiation. In addition to the hexaboride class of materials, another heavily researched group of materials for NIR blocking is based upon tungsten oxides [47,169,170], namely, cesium tungsten bronze [101,170] and potassium tungsten bronze [171]. Cesium and potassium tungsten bronze nanoparticle-based coatings have absorption peaks in the 1200–1500 nm range, while the tungsten oxide range has peaks from 600–1500 nm, depending upon the level of oxygen reduction [47]. The use of sodium tungsten bronze [47] can result in blueshifts into wavelengths ranging from 900–1200 nm, which may be desirable as compared to the other combinations of tungsten bronze.

While passive window coatings can result in energy savings from absorbing solar NIR during summer operation, they prevent useful solar heating during the winter season. As such, dynamically controlling the blocking of this portion of the spectrum represents an attractive method for reducing a building's energy demand throughout the entire year [172]. The primary approaches for this have been electrochromic (electric-charge-induced changes) or thermochromic (temperature-based color changes) coatings, which can also now be achieved with nanoparticles. The primary material for thermochromic changes is vanadium oxide, which has a reversible structural transformation from metallic to semiconducting states at the material's Mott transition temperature [173]. In the typical thin-film mode, the change in solar transmittance is around 10%, but this film comes with a limited visible transmittance to ∼40%. Nanoparticles suspended in a dielectric host, on the other hand, can achieve changes in solar transmittance from 10%–20% and could maintain a visible transmittance exceeding 50% [173]. While thermochromic windows are attractive due to their passive nature, the ability to actively control the transmittance is also promising from an energy savings perspective, but they tend to suffer from long switching times [172]. To overcome this limit, the Milliron group has been leading the way in using plasmonic nanocrystals that exhibit shifting in plasmon resonance when a charge is applied to the particles when suspended in an electrolyte [174,175]. Their work has shown the high degree of sensitivity of the plasmon resonance in the NIR due to particle shape [176], doping [175,177], and dopant distribution [92]. As the plasmon peak is sensitive to the free-electron content provided by the dopants, embedding these particles in an electrolyte where the charge density near the particle can be actively controlled by an applied potential results in an ability to significantly modify the plasmon resonance (and impact the overall magnitude). The most exciting part of this technology is that changes to plasmon resonance of these particles has minimal impact on the visible transmittance (of the order of 90%), but causes drastic changes to the NIR

transmittance (controllable from 20%–80%) [174,178]. Figure 14 illustrates the concept by increasing free charge carriers on ITO thin film through applied voltage.

5.2b. Selective Scattering

Applications in Photonic Crystals. Solid-state nanoparticle arrays arranged at an interface have been explored as a means to selectively control the propagation of particular wavelengths of light. This has been done for light traversing normally or transversely to the interface. Normal irradiance produces Bragg interference for selective, narrowband filtration, while transverse irradiance produces photonic bandgaps that suppress particular wavelengths of light from traveling through. Both of these effects are based on collective light scattering, which is controlled through modification of the array geometry and the properties of the individual nanoparticle constituents.

Periodically arranged nanoparticles on an interface have been shown to support a narrow, selective light filtration. The individual nanoparticles in the lattice act as dipole antennae scatterers; and electrons in the nanoparticles oscillate with the incident electric field. With normal irradiance, the polarization of light is in-plane with the nanoparticle array. The scattered light is directed radially away from each nanoparticle with an angle-dependent amplitude that follows $\sin^2(\theta)$, where θ is the angle with respect to the polarization of the incident light. When the incident light matches the lattice constant of the nanoparticle array, the scattered light is in-phase with the incident light, causing an enhanced electron oscillation, and thus scattering is increased, as shown in Fig. 15. The net effect is increased scattering when incident wavelengths are multiples of the geometric arrangements of the nanoparticles. This effect has been suggested for telecommunication multiplexing applications, in which the nanoparticle geometry can define narrowband filtration of particular wavelength of light [179].

For scattering to occur at wavelengths corresponding to the geometry of the array, the plasmon resonance must be close to, but redshifted from, the lattice constant. This is a result of the creation of a Fano resonance between the broadband plasmon mode and the narrowband lattice diffraction. The diffraction modes result from geometric

Figure 14

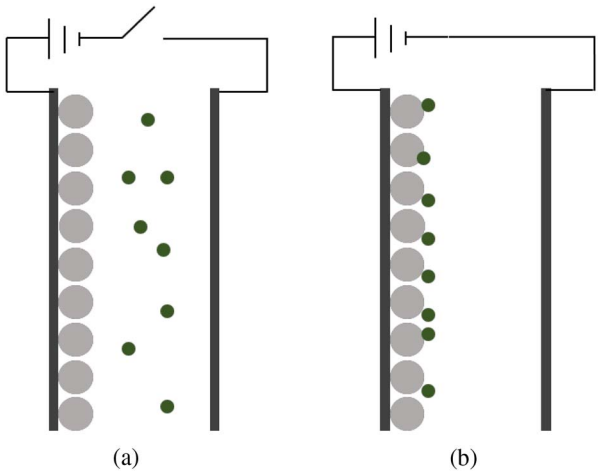

Window with changing optical properties through turning on and off a voltage, changing the carrier concentration. The figure shows, when voltage is (a) off and (b) on, directing ions in the electrolyte to the ITO.

features of the lattice. For example, in an infinite square array of nanoparticles, each unique line of nanoparticles causes constructive interference to occur. The two primary diffraction modes that appear are the axial and diagonal. For a square lattice with a lattice constant D, the axial diffraction occurs at wavelengths near D, and the diagonal diffraction occurs at wavelengths near $\sqrt{2}D$. Constructive interference also occurs at linear factors of the geometric diffraction modes, since two wavelengths between neighboring particles still have scattered light in-phase with the incident light. However, these higher order diffraction modes are typically at wavelengths below the plasmon wavelengths and do not produce significant light filtration. The interaction between the broad plasmon and narrow diffraction modes generates an asymmetric Fano resonance profile. Optimization of the narrowband Fano resonance involves changes to the lattice geometry, the nanoparticle unit cells of the lattice, and the interface materials.

A plot showing the transmission spectra of a square lattice consisting of 80 nm Au nanoparticles with normal incidence is shown in Fig. 16. The spectra were computed using the coupled dipole approximation (CDA) by treating each nanoparticle as a point dipole and computing the scattering effects over the entire lattice [51,180,181]. It is noted that there is a dip in the transmission observed in the figure that is centered at 708 nm and has a full width at half-maximum (FWHM) of 28 nm. There is also a dip in transmission located at 525 nm, which is a combination of the plasmon

Figure 15

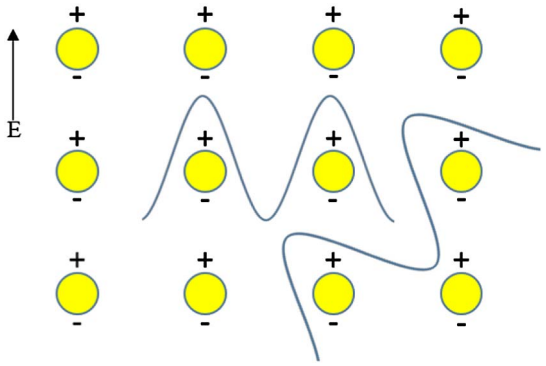

Illustration of a nanoparticle array with light incident normal to the lattice and polarized along the y direction. Scattering from particles axially along x and diagonally are shown in the figure, illustrating the different wavelengths required for the scattered light to be in phase with incident light.

Figure 16

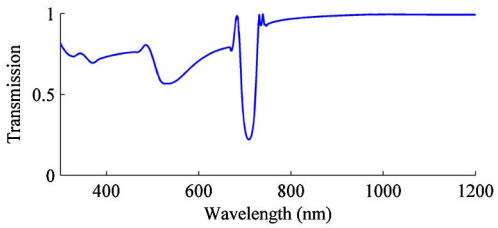

Calculated transmission through a square array of 80 nm diameter gold nanoparticles with a lattice constant of 700 nm.

resonance from the Au nanoparticles and the diffraction mode from half the diagonal length, which is 495 nm. Since the half-diagonal is smaller than the plasmon resonance, the cumulative scattering effects are minimized and the peak is significantly smaller than the primary diffraction peak from axial nanoparticle coupling.

Several lattice types have been considered to generate the narrow Fano resonance for light filtration. A square array is the simplest to fabricate and analyze. Since all particles contribute to the coupling that is involved in the lattice to generate the sharp extinction peak, it turns out that the transmission spectra are independent of the light polarization for normal incidence. This is not true for rectangular arrays. Since the scattering amplitude scales by $\sin(\theta)$, particles do not scatter in-line with the polarization of the incident light. As a result, lattice dimensions for light scattered from "neighboring" particles changes as polarization angle is changed. The primary lattice configurations that have been optimized include square, rectangular, and hexagonal arrangements.

Metal particles have typically been analyzed when optimizing nanoparticle arrays for selective filtration. This is a result of the need to have significant plasmon decay into scattering and to have a resonance that is redshifted from the lattice dimensions. Metals can be readily fabricated at large sizes and work well with traditional lithography techniques, such as photolithography, electron beam lithography, and nanoimprint lithography. Gold nanoparticles have been almost exclusively used due to their long-term stability from oxidation resistance and a plasmon resonance location that is around 600–800 nm, depending on the size of the nanoparticle.

The interface materials have been shown to play an important role in the optimization of nanoparticle arrays for selective filtration. Since the narrowband filtration of light is based on scattering, the lattice constant of the array has to be larger than the plasmon wavelength. This is because wavelengths shorter than the plasmon wavelength simply pass through the particle with no plasmonic absorption. Previous works have shown that, optimally, the geometry of the array should have dimensions larger than, but near to, the plasmon resonance to have enhanced light filtration [51,54,180,182]. The opposite effect is seen with thin metal sheets with arrays of holes. Based on Babinet's principle, if narrowband light scattering occurs with nanoparticle arrays, narrowband transmission through thin metal films occurs with nanohole arrays [183]. In this way, both narrowband extinction or transmission of light through an interface is possible and tunable using nanoparticle or nanohole arrays, respectively.

Applications in Solar Energy Systems. Just as particle–liquid suspensions are being investigated for applications in solar energy systems, thin-film coatings with nanoparticles imbedded in them can also be used for solar energy applications. It should be noted that these coatings may not be optically selective by themselves, but within the *system* they are designed to retain parts of the solar spectrum that otherwise may have been lost. Since there has been an extremely large number of theoretical and experimental papers on solar cell light trapping, there have already been a number of review papers that cover this field in detail, e.g., [184,185]. The basic concept for this field was formalized by Yablonovitch and Cody [186], who estimated that a textured photovoltaic surface could increase the effective absorption inside the cell (due to total internal reflection and a greatly increased internal path length) by up to $4n^2$ (or $\sim 50\times$ for silicon cells), although absorption increases of the order of $5\times$ are more realistic [187]. This enhancement enables a well-designed system to have higher performance while, at the same time, using less material (read: cheaper). To influence the incident spectrum, of course, this roughness must be on the micrometer to submicrometer scale. Early attempts to achieve this enhancement relied on texturing and patterning of the cell's surface, e.g., [188,189]. More recently the inclusion of

nanoparticles (sometimes in combination with patterning/texturing [190]) has been rapidly developing—see the reviews Atwater and Polman [185], Guo *et al.* [191], or Spinellii *et al.* [184]. As was discussed by Smith *et al.* [192], there are three main ways to achieve enhancement in a photovoltaic cell embedded with nanoparticle (shown in Fig. 17). As discussed above, depositing or embedding nanoparticles near the surface roughness enables enhanced absorption. Nanoparticles can also be included in the active layer of the cell to enhance the electronic near fields. As another mode of enhancement, nanoparticles can be included near the backreflector to obtain diffuse reflection and to generate surface plasmon polaritons.

In the first category, several researchers have focused on the analysis of single particles (typically silver) embedded in a dielectric in close proximity to a bulk substrate as a means to trap light in thin-film solar cells [185,193–196]. Since fabrication represents much of the challenge, there are a number of studies that describe methods for self-assembly of the nanoparticles in the cells [196], deposition methods [187], and other synthesis and fabrication approaches [197]. One application by Buonsanti *et al.* utilizes colloidal gold particles that have been wet-coated in an array as part of a backreflector that achieves high diffuse reflectance [198]. In the second category of PV enhancement, the strong near-field plasmon resonance can be used to enhance local optical electric fields and can give rise to >50% effective absorption enhancement [199,200]. In the third category of enhancement, the nanoparticles can be located on the backreflector to scatter light back into the cell. According to Beck *et al.* this can "enhance the external quantum efficiency of thin Si solar cells by a factor of 2.3 at this wavelength where transmission losses are prevalent" [187]. Although these techniques have been mostly limited to laboratory-scale cell testing, the meteoric increase in commercial sales of photovoltaics provides a big incentive to pull this type of enhancement into modules. As is shown in Table 3, however, it is clear that there are still a large number of competing ideas as to the best mechanism/approach for employing nanoparticles in photovoltaic devices.

While usage for light trapping is thoroughly investigated, others are investigating approaches for bandpass filters and reflective mirror optics for use in solar systems. Smirnov *et al.* developed a nanostructured mirror for reflecting UV light through controlled layer-by-layer deposition of ZrO_2 and SiO_2 colloidal suspensions [205]. O'Brien *et al.* created selective transparent films with high reflectance between

Figure 17

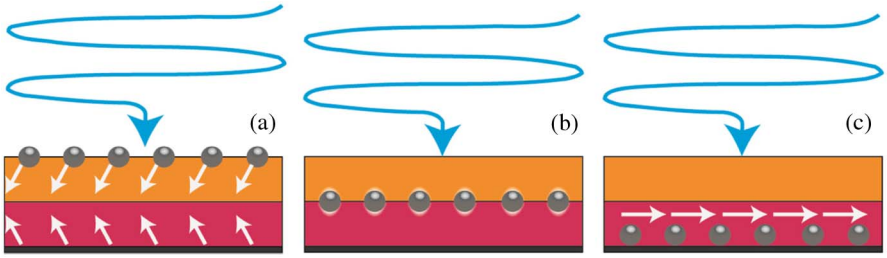

Potential PV improvements with embedded nanoparticles. A, scattering at the top surface to increases the path length of light in the cell. B, placing plasmonic nanoparticles at the active layer to enhance electric near fields, and potentially absorbance; C, on the back-side to achieve scattered reflection and/or surface plasmon polaritons [192]. Reprinted from Smith *et al.*, "Plasmon resonances for solar energy harvesting: a mechanistic outlook," Nano Today **10**(1), 67–80. Copyright 2015, with permission from Elsevier.

Table 3. Selected Studies of Plasmonic Enhancement in Photovoltaics

Nanoparticle Location in Cell	Nanoparticle Diameter (nm), Material(s), Morphology	Active Wavelength Range (nm)	Analysis Method	Reference
Backscattering layer	~100–300, Ag, spheres	520–1100	Experiment	[196]
Backscattering layer	100–200, Au, spheres	550–1300	Experiment	[159]
Backscattering layer/active layer (DSC)	100–700, Ag, spheres (larger were better)	550–800	Model	[201]
Active layer	5–30, Ag, spheres (and dielectric shells)	550–800	Model (Mie theory)	[200]
Active layer	10–20, Ag, spheres	300–700	Experiment	[202]
Front/backscattering layer	100–200, Ag, spheres	400–1200	Model and experiment	[187]
Front-scattering layer	50–300, Al, spheres	300–1200	Model	[203]
Front-scattering layer	~100, Al sphere on graphene sheets	280–1000	Experiment	[204]

500 and 700 nm through the alternating methods of spin-coating silica nanoparticles and sputter-coating ITO thin films [206]. This is an interesting approach of combining conventional thin-film techniques with that of nanoparticle thin films.

An additional, more recent approach for the use of selective scattering is for the enhanced growth of algae and biomass productions using plasmonic reflectors. All of these approaches propose to enhance the amount of light that can be backscattered into the algae to enhance growth. Nanoparticle selection is based upon achieving high scattering for a wavelength that corresponds to high absorption for a given algae species. Ooms *et al.* demonstrated an up to 6.5% increase in growth rate of biomass by using an array of gold nanodisks [207]. The approach also demonstrated that a significant portion of nonphotosynthetically active light was transmitted through the sample, which could be used in other components. Torkamani *et al.* demonstrated that enhanced algal growth of 30% could be achieved by placing 50 nm silver nanoparticles after the algae [208]. Their research group extended this work by developing a polymer film with embedded plasmonic nanoparticles, where an enhancement of 25% in biomass production was demonstrated [209]. A similar approach was taken with gold and silver nanoparticles placed around growth flasks, which resulted in increased formation of photopigments [210].

5.2c. Selective Emission

Selective emission in a thin film involves embedding nanoparticles in the film (or bonding them with a substrate) to achieve controlled thermal (blackbody), photoluminescent, or phosphorescent emission in thin film or on a substrate. In many cases, multiple nanoparticles are used and/or the nanoparticles of interest form one part—albeit a critical part—of the larger optical system. Thus, selective emission often involves a relatively more complicated design/architecture than selective absorption or scattering systems.

Although long wavelength thermal emission is considered to be an energy loss to be minimized in many applications, it is also possible to make nanomaterials that selectively emit within the "atmospheric window" to provide cooling for an application. The atmospheric window is characterized by gaps in where CO_2 and H_2O absorb long wavelengths, namely, between 8 and 13 μm and 20 and 30 μm. In a study by Rephaeli *et al.* [18], a metal–dielectric structure was fabricated that can selectively emit in this window. The system consists of several bilayers of 25–105 nm thickness, made of TiO_2 and MgF_2, topped with a SiC layer and a structured quartz layer [18]. While not technically consisting of nanoparticles, the cost/performance of this type of system might be improved with embedded nanoparticles. The idea of using small particles to enhance the radiative cooling of thin films was pioneered by the work of Nilsson and Niklasson, who focused on the use of pigmented polyethylene foils

to enhance the cooling effect [211]. The pigments studied were 100 μm particles of ZnS, ZnSe, TiO_2, ZrO_2, and ZnO with the best performance achieved by the ZnS foil. This work was extended with nanoparticles for enhanced thermal emission in the atmospheric window, which was pioneered by Gentle and Smith [212]. They were able to demonstrate subambient radiative cooling from a film doped with a mixture of silica and SiC nanoparticles. The only other related study investigated the difference between metal and polar nanoparticles embedded in thin films from the visible to the IR [213]. The primary result is that the inclusion of BN particles (polar material) leads to additional peaks in the host material (SiC) that are not attributable to either the particle or film. A similar effect is observed for Au nanoparticles introduced into a polyethylene film, albeit in the visible and NIR wavelength ranges. Further, the authors note that the emittance properties depend on volume fraction and size for the metal particles (as the surface plasmon is size dependent), while the properties for polar materials have no size dependence.

As spectral conversion (emission) approach the flat plate luminescent concentrator represents an interesting application. To date, quantum dots and organic dyes are typically used in these applications [214,215], but selectively scattering nanoparticles could also provide an interesting concentrator alternative. A "standard" luminescent concentrator consists of a highly transparent sheet of material (plastic or glass) that has quantum dots and/or organic dyes embedded throughout. When sunlight hits from above, the particles and/or dyes absorb the incoming light and then re-emit at a lower energy level (e.g., downconversion). For photovoltaic applications, PV cells are placed around the edges of the sheet, and the bandgap of the cell will be chosen to match with the spectrum of emission (as is shown in Fig. 18). If the transparent medium is of a high refractive index, most of this light will be totally internally reflected and guided to the sides of the material. Depending on the aspect ratio and the losses in the system, the light output at the sides will be concentrated by some ratio X. Although the concentration ratio, X, is rarely $\gg 1$, the reduction in photovoltaic area and elimination of tracking in the system may enable cost reductions.

Large field emitters based on nanoparticles can be used to produce a new generation of low-power, flat-panel displays. Much of the work in this area relies on various carbon nanotubes, and in particular on how to order nanotubes into a coherent, dense structure. Some examples are the work of Choi *et al.* [216], who proposed that SWCNTs emitters can be deposited via electrophoresis onto a patterned microstructure. In a different approach, Sohn *et al.* [217] produced large field emitters (4×10^{-5} cm^2, shown in Fig. 19) by first depositing Fe nanoparticles on a patterned Si substrate, then growing MWCNTs from the bottom up. With these and other preparation methods [218,219], bright emission can be achieved.

An application with large commercial potential, selective nanoparticle emission can be used to fabricate light-emitting diodes (LEDs). The nanomaterials used for these applications has a semiconductor base material that is doped or mixed with metals.

Figure 18

Luminescent concentrator schematic.

In a study by Zeng *et al.* [220], hollow ZnO nanoparticles decorated with Au and Pt were found to have potential as blue LEDs, due to their high blue UV photoluminescence relative to pure ZnO nanoparticles. The photoluminescent intensity spectra of these materials are shown in Fig. 20.

Riley *et al.* [221] used quantum wells and nanowires of GaN/InGaN to create LED arrays that can be tuned to achieve emission between 365 and 700 nm, depending on their fabrication. If broadband emission can be achieved in one device, it may be possible to fabricate white LEDs.

Another application of selective emission is for the enhancement of photosynthetic activities, such as algal production or artificial photosynthesis. In the past, this has been primarily achieved with molecular dyes, powders, and on luminescent paints [222,223]. Recently, this approach has been extended to systems using upconverting

Figure 19

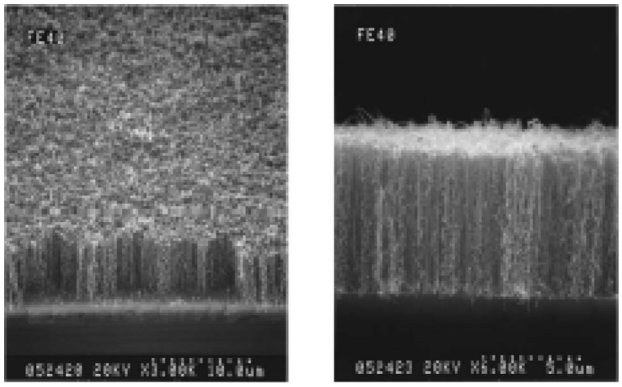

Scanning electron micrographs of a carbon nanotube array, which have been proposed as large area field emitters by Sohn *et al.* [217]. Reprinted with permission from Sohn *et al.*, Appl. Phys. Lett. **78**, 901–903 (2001) [217]. Copyright 2001 AIP Publishing LLC.

Figure 20

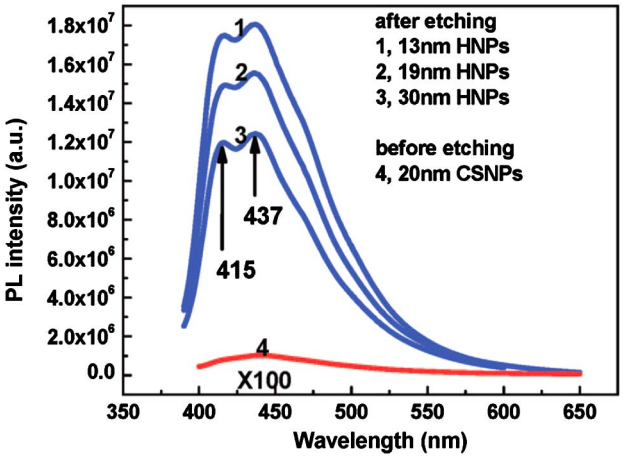

Photoluminescence spectra of hollow ZnO nanoparticles with different diameters [220]. Reprinted (adapted) with permission from Zeng *et al.*, ACS Nano **2**, 1661–1670 (2008) [220]. Copyright 2008 American Chemical Society.

or downconverting nanoparticles, although the number of demonstrations with actual algal growth is rather limited. The work by Wondraczek *et al.* noted the potential use of nanoparticles for artificial and natural photosynthesis, but no results of enhancement to growth were presented [224] among many other articles devoted to the process and optical spectra of upconverting and downconverting nanoparticles; key reviews cover the details of such particles [225–227]. A proposed system arrangement of using spectral conversion with nanoparticles for enhanced algae growth is show in Fig. 21, with experiments ongoing. A similar approach is covered by a U.S. patent for wastewater treatment and enhanced photosynthesis. Layers of downconverting quantum dots and upconverting nanoparticles sandwich a layer of algae [228].

5.2d. Selective Hot Electron Transfer

Nanoparticles that selectively convert photons into plasmons can also have the plasmon decay into an electron to an adjacent material. This has been applied to catalysis, PV systems, and tunable photodetectors [229]. These applications utilize light absorbed by the nanoparticle as an electron to be used by an adjacent material. Applications involving catalysis are not utilized as selective absorbers and are not discussed in detail in this work.

Applications have been proposed to incorporate nanoparticles for selective hot electron transfer in PV systems. Electrons generated in nanomaterials due to plasmon decay have been recently utilized in selective photodetection. In these applications, nanostructures are fabricated on a material such as graphene, which acts as the hot electron acceptor. When a voltage is applied across the material, the hot electron transferred from the nanoparticle to the adjacent material can be collected as photocurrent. The choice of nanoparticle composition and size allows control over which photons are converted to photocurrent through the generated plasmon. Recent works have shown this concept and characterized the efficiency of the conversion of photons to electrons through nanoparticles. Gold nanoparticles grown lithographically on graphene have been utilized and shown to generate a transfer of electron to the graphene with an external quantum efficiency (EQE) between 10% and 22% in terms of the conversion from plasmon to electron [29,230,231]. This has also been observed for CdSe nanoparticles on a TiO_2 thin film, in which selective absorption in the semiconductor nanoparticles decays as electrons into the adjacent film with an EQE of 12% [232,233]. Additionally, silicon nanoparticles have been explored for multiple

Figure 21

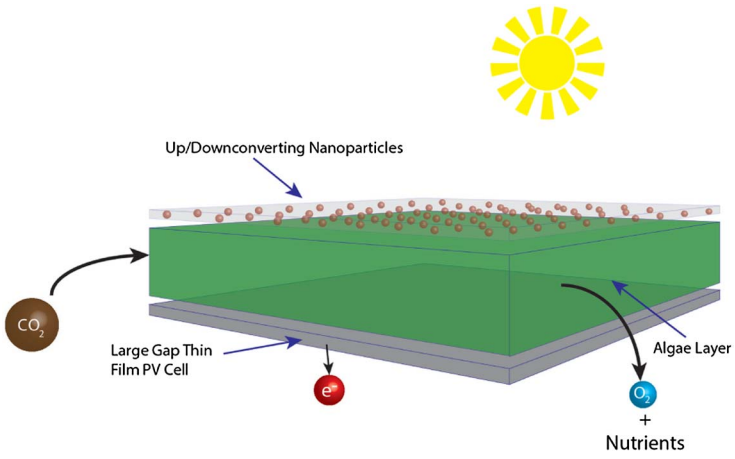

Proposed system for enhanced algae production using selective emission nanoparticles.

Table 4. Comparison among Selected Applications

Application	Nanoparticle Material(s)/ Morphology	Active Wavelength Range (nm)	Type of Study	Reference(s)
Hybrid solar thermal/PV collectors	Polypyrrole/spheres	300–1400	0.01 m^2 outdoor test nonflowing	[153]
	Silica/spheres	300–550	Model, test of optical properties	[154]
	Silver/plates Carbon/nanotubes	400–700 200–1200	Model, benchtop test nonflowing	[152]
	Gold–silica/core–shell; silver–silica/core–shell; silver/spheres	750–1200 800–1500 300–500	Numerical modeling	[150,151,235]
	ITO/nanocrystal; gold/nanorods; gold/spheres	1600–2500 780–2500 400–600	Optical properties testing up to 300°C	[62,98]
Sunscreens	Zinc oxide/spheres; titanium oxides/spheres	315–400 280–315	Commercial sunscreens	[157]
Passive window coatings	Hexaborides/spheres	700–1500	Lab testing	[104]
	Tungsten oxides/spheres	700–1600	Lab testing	[47,99,100,169–171,236]
Thermochromic window coatings	Vanadium oxide/spheres; vanadium oxide/ellipses	1500–3000 1000–2000	Lab testing	[173]
Electrochromic window coatings	ITO/nanocrystals	1600–2500	Commercial development underway	[172,175]
Thin-film photovoltaics	Gold/spheres; silver/spheres	500–600 350–450	Lab testing	[184,195,196]
UV mirrors	Zirconium oxide + silica/spheres; silica/spheres	500–700 200–400	Lab testing	[205,206]

exciton generation [234]. For these applications, photons with energies greater than twice the bandgap can be split into two electron–hole pairs as opposed to thermalization of excess energy. More work is required to determine optimization parameters for use in selective absorption of light with high conversion efficiencies.

5.3. Nanomaterials: Where Do We Go from Here?

From the wide variety of optical selectivity highlighted above, it can be seen that nanoparticles are poised to move from the laboratory and into solar collectors, medicine, buildings, and a myriad of other real-world applications in the near future. Although a very diverse range of potential applications is possible, only a limited amount of the nearly unlimited potential combinations of materials, particle sizes, and morphologies has been explored (as can be seen in the selected studies shown in Table 4). Additionally, little progress has been made toward optimizing nanoparticles for their applications. In terms of practical implementation, methods for scaling up the production of nanomaterials to real applications are in their infancy, particularly for composite particles. In addition, very few studies discuss the reliability of these materials over their lifespans or how to handle them at the end of their lives. Some particular research areas still offer significant opportunity for future study, in particular the ability to control or enhance thermal emission, the coupling of light with thermal and electrical processes, and understanding the long-term behavior of nanoparticles in real systems. Additionally, many groups have started early exploration into how to dynamically control optical properties through different mechanisms. This could lead to new and novel approaches to control a wide range of processes heretofore not explored.

6. CONCLUSIONS

Nanoparticles present an attractive and low-cost method for achieving selective spectral filtration. Because of the development of many facile synthesis techniques that can be used to grow nanoparticles of different materials, shapes, and sizes, the spectral properties can be readily tuned and scaled up to large volume production. Additionally, the relatively small amount of nanoparticles required to achieve significant absorption results in low cost. While metallic nanoparticles have demonstrated a large level of tuning in the visible range through particle size and morphology, semiconducting nanoparticles offer tunability in the IR region. At this point, nanoparticles as selective spectral absorbers in fluids are being pursued primarily in research applications, particularly in solar energy applications. However, many demonstration projects are coming to fruition in the near term that will likely enable larger-scale commercial developments. The use of selective nanoparticle absorption and scattering, used in thin film applications, has proven beneficial for the development of thinner solar cells and more effective sunscreens. Another exciting feature of nanoparticles over other optical filtration technologies is that they can serve as building blocks for multiple applications. For example, we presented approaches here in which the particles can either be dispersed in a fluid or applied as a thin film. If dispersed in a fluid, they can potentially be mixed, separated, and pumped in and out of an application. While commercial products are limited primarily to paints and sunscreens at this point, it appears that new products may be forthcoming that utilize the unique optical advantages afforded by nanoparticles.

FUNDING

Advanced Research Projects Agency Energy (ARPA-E) (DE-AR0000463); Australian Renewable Energy Agency (ARENA) (USO-1 MUSIC); Australian

Research Council (ARC) (DECRA DE160100131); National Aeronautics and Space Administration (NASA) (NNX15AM75A).

ACKNOWLEDGMENT

We thank the University of Tulsa and the University of New South Wales for the use of their equipment, facilities, and support for this research.

REFERENCES

1. N. Gat, "Imaging spectroscopy using tunable filters: a review," Proc. SPIE **4056**, 50–64 (2000).
2. M. A. C. Chendo, M. R. Jacobson, and D. E. Osborn, "Liquid and thin-film filters for hybrid solar energy conversion systems," Sol. Wind Technol. **4**, 131–138 (1987).
3. Z. J. Yu, K. C. Fisher, B. M. Wheelwright, R. P. Angel, and Z. C. Holman, "PVMirror: a new concept for tandem solar cells and hybrid solar converters," IEEE J. Photovolt. **5**, 1791–1799 (2015).
4. R. Winston, E. Yablonovitch, L. Jiang, B. K. Widyolar, M. Abdelhamid, G. Scranton, D. Cygan, and A. Kozlov, "Hybrid solar collector using nonimaging optics and photovoltaic components," Proc. SPIE **9572**, 957208 (2015).
5. A. Mojiri, R. Taylor, E. Thomsen, and G. Rosengarten, "Spectral beam splitting for efficient conversion of solar energy—a review," Renew. Sust. Energy Rev. **28**, 654–663 (2013).
6. S. J. Madsen, M. S. Patterson, and B. C. Wilson, "The use of India ink as an optical absorber in tissue-simulating phantoms," Phys. Med. Biol. **37**, 985–993 (1992).
7. W. G. van Sark, J. de Wild, J. K. Rath, A. Meijerink, and R. E. Schropp, "Upconversion in solar cells," Nanoscale Res. Lett. **8**, 81 (2013).
8. A. Shalav, B. S. Richards, and M. A. Green, "Luminescent layers for enhanced silicon solar cell performance: up-conversion," Sol. Energy Mater. Sol. Cells **91**, 829–842 (2007).
9. C. Strümpel, M. McCann, G. Beaucarne, V. Arkhipov, A. Slaoui, V. Švrček, C. del Cañizo, and I. Tobias, "Modifying the solar spectrum to enhance silicon solar cell efficiency—an overview of available materials," Sol. Energy Mater. Sol. Cells **91**, 238–249 (2007).
10. C. Fabry and A. Perot, "Theorie et applications d'une nouvelle methode de spectroscopie interferentielle," Ann. Chim. Phys. **16**, 115 (1899).
11. F. Crisostomo, R. A. Taylor, T. Zhang, I. Perez-Wurfl, G. Rosengarten, V. Everett, and E. R. Hawkes, "Experimental testing of SiN_x/SiO_2 thin film filters for a concentrating solar hybrid PV/T collector," Renew. Energy **72**, 79–87 (2014).
12. C. Shou, Z. Luo, T. Wang, W. Shen, G. Rosengarten, W. Wei, C. Wang, M. Ni, and K. Cen, "Investigation of a broadband TiO_2/SiO_2 optical thin-film filter for hybrid solar power systems," Appl. Energy **92**, 298–306 (2012).
13. F. Crisostomo, R. A. Taylor, D. Surjadi, A. Mojiri, G. Rosengarten, and E. R. Hawkes, "Spectral splitting strategy and optical model for the development of a concentrating hybrid PV/T collector," Appl. Energy **141**, 238–246 (2015).
14. A. P. Raman, M. A. Anoma, L. Zhu, E. Rephaeli, and S. Fan, "Passive radiative cooling below ambient air temperature under direct sunlight," Nature **515**, 540–544 (2014).
15. A. Q. Liu, W. M. Zhu, D. P. Tsai, and N. I. Zheludev, "Micromachined tunable metamaterials: a review," J. Opt. **14**, 114009 (2012).
16. M. Wegener, "Photonic metamaterials and transformation optics: a very brief introduction and review," in *Nano-Optics for Enhancing Light-Matter*

Interactions on a Molecular Scale: Plasmonics, Photonic Materials and Sub-Wavelength Resolution (Springer, 2013), pp. 23–28.
17. C. M. Soukoulis and M. Wegener, "Past achievements and future challenges in the development of three-dimensional photonic metamaterials," Nat. Photonics **5**, 523–530 (2011).
18. E. Rephaeli, A. Raman, and S. Fan, "Ultrabroadband photonic structures to achieve high-performance daytime radiative cooling," Nano Lett. **13**, 1457–1461 (2013).
19. H. Wang, V. Prasad Sivan, A. Mitchell, G. Rosengarten, P. Phelan, and L. Wang, "Highly efficient selective metamaterial absorber for high-temperature solar thermal energy harvesting," Sol. Energy Mater. Sol. Cells **137**, 235-242 (2015).
20. C. F. Guo, T. Sun, F. Cao, Q. Liu, and Z. Ren, "Metallic nanostructures for light trapping in energy-harvesting devices," Light Sci. Appl. **3**, e161 (2014).
21. J. B. Chou, Y. X. Yeng, A. Lenert, V. Rinnerbauer, I. Celanovic, M. Soljačić, E. N. Wang, and S.-G. Kim, "Design of wide-angle selective absorbers/emitters with dielectric filled metallic photonic crystals for energy applications," Opt. Express **22**, A144–A154 (2014).
22. Q. Huang, J. Wang, B. Quan, Q. Zhang, D. Zhang, D. Li, Q. Meng, L. Pan, Y. Wang, and G. Yang, "Design and fabrication of a diffractive optical element as a spectrum-splitting solar concentrator for lateral multijunction solar cells," Appl. Opt. **52**, 2312–2319 (2013).
23. M. Stefancich, A. Zayan, M. Chiesa, S. Rampino, L. Kimerling, and J. Michel, "Single element spectral splitting solar concentrator for multiple cells CPV system," Opt. Express **20**, 9004–9018 (2012).
24. B. Fisher and J. Biddle, "Luminescent spectral splitting: efficient spatial division of solar spectrum at low concentration," Sol. Energy Mater. Sol. Cells **95**, 1741–1755 (2011).
25. L. R. Bradshaw, K. E. Knowles, S. McDowall, and D. R. Gamelin, "Nanocrystals for luminescent solar concentrators," Nano Lett. **15**, 1315–1323 (2015).
26. R. K. Kostuk and G. Rosenberg, "Analysis and design of holographic solar concentrators," Proc. SPIE **7043**, 70430I (2008).
27. M. B. Cortie and A. M. McDonagh, "Synthesis and optical properties of hybrid and alloy plasmonic nanoparticles," Chem. Rev. **111**, 3713–3735 (2011).
28. G. Mie, "Contributions on the optics of turbid media, particularly colloidal metal solutions," Ann. Phys. **330**, 377–445 (1908).
29. D. DeJarnette and D. K. Roper, "Electron energy loss spectroscopy of gold nanoparticles on graphene," J. Appl. Phys. **116**, 054313 (2014).
30. P. Offermans, M. C. Schaafsma, S. R. K. Rodriguez, Y. Zhang, M. Crego-Calama, S. H. Brongersma, and J. Gómez Rivas, "Universal scaling of the figure of merit of plasmonic sensors," ACS Nano **5**, 5151–5157 (2011).
31. C.-Y. Tsai, S.-P. Lu, J.-W. Lin, and P.-T. Lee, "High sensitivity plasmonic index sensor using slablike gold nanoring arrays," Appl. Phys. Lett. **98**, 153108 (2011).
32. C. Kojima, Y. Watanabe, H. Hattori, and T. Iida, "Design of photosensitive gold nanoparticles for biomedical applications based on self-consistent optical response theory," J. Phys. Chem. C **115**, 19091–19095 (2011).
33. D. Pissuwan, S. M. Valenzuela, and M. B. Cortie, "Therapeutic possibilities of plasmonically heated gold nanoparticles," Trends Biotechnol. **24**, 62–67 (2006).
34. S. Yamashita, H. Fukushima, Y. Niidome, T. Mori, Y. Katayama, and T. Niidome, "Controlled-release system mediated by a retro Diels-Alder reaction induced by the photothermal effect of gold nanorods," Langmuir **27**, 14621–14626 (2011).

35. T. Niidome, M. Yamagata, Y. Okamoto, Y. Akiyama, H. Takahashi, T. Kawano, Y. Katayama, and Y. Niidome, "PEG-modified gold nanorods with a stealth character for in vivo applications," J. Control. Release **114**, 343–347 (2006).
36. B. Roy, M. Arya, P. Thomas, J. K. Jurgschat, K. V. Rao, A. Banerjee, C. M. Reddy, and S. Roy, "Self-assembly of mesoscopic materials to form controlled and continuous patterns by thermo-optically manipulated laser induced microbubbles," Langmuir **29**, 14733–14742 (2013).
37. T. Uwada, S. Fujii, T. Sugiyama, A. Usman, A. Miura, H. Masuhara, K. Kanaizuka, and M. Haga, "Glycine crystallization in solution by cw laser-induced microbubble on gold thin film surface," Appl. Mater. Interfaces **4**, 1158–1163 (2012).
38. S. Fujii, K. Kanaizuka, S. Toyabe, K. Kobayashi, E. Muneyuki, and M. Haga, "Fabrication and placement of a ring structure of nanoparticles by a laser-induced micronanobubble on a gold surface," Langmuir **27**, 8605–8610 (2011).
39. Y. Nishimura, K. Nishida, Y. Yamamoto, S. Ito, S. Tokonami, and T. Iida, "Control of submillimeter phase transition by collective photothermal effect," J. Phys. Chem. C **118**, 18799–18804 (2014).
40. M. Lisunova, X. Wei, D. DeJarnette, G. T. Forcherio, K. R. Berry, P. Blake, and D. K. Roper, "Photothermal response of the plasmonic nanoconglomerates in films assembled by electroless plating," RSC Adv. **4**, 20894–20901 (2014).
41. D. DeJarnette, T. Otanicar, N. Brekke, P. Hari, K. Roberts, A. E. Saunders, and R. Morad, "Plasmonic nanoparticle based spectral fluid filters for concentrating PV/T collectors," Proc. SPIE **9175**, 917509 (2014).
42. A. O. Govorov, W. Zhang, T. Skeini, H. Richardson, J. Lee, and N. A. Kotov, "Gold nanoparticle ensembles as heaters and actuators: melting and collective plasmon resonances," Nanoscale Res. Lett. **1**, 84–90 (2006).
43. A. O. Govorov and H. H. Richardson, "Generating heat with metal nanoparticles," Nano Today **2**(1), 30–38 (2007).
44. A. Kosuga, Y. Yamamoto, M. Miyai, M. Matsuzawa, Y. Nishimura, S. Hidaka, K. Yamamoto, S. Tanaka, Y. Yamamoto, S. Tokonami, and T. Iida, "A high performance photothermal film with spherical shell-type metallic nanocomposites for solar thermoelectric conversion," Nanoscale **7**, 7580–7584 (2015).
45. F. Scotognella, G. Valle, A. R. Srimath Kandada, M. Zavelani-Rossi, S. Longhi, G. Lanzani, and F. Tassone, "Plasmonics in heavily-doped semiconductor nanocrystals," Eur. Phys. J. B **86**, 154 (2013).
46. J. A. Faucheaux, A. L. D. Stanton, and P. K. Jain, "Plasmon resonances of semiconductor nanocrystals: physical principles and new opportunities," J. Phys. Chem. Lett. **5**, 976–985 (2014).
47. H. Takeda and K. Adachi, "Near infrared absorption of tungsten oxide nanoparticle dispersions," J. Am. Ceram. Soc. **4061**, 4059–4061 (2007).
48. W. Doyle, "Optical properties of a suspension of metal spheres," Phys. Rev. B **39**, 9852–9858 (1989).
49. A. Mary, D. Koller, A. Hohenau, J. Krenn, A. Bouhelier, and A. Dereux, "Optical absorption of torus-shaped metal nanoparticles in the visible range," Phys. Rev. B **76**, 245422 (2007).
50. D. DeJarnette, J. Norman, and D. K. Roper, "Spectral patterns underlying polarization-enhanced diffractive interference are distinguishable by complex trigonometry," Appl. Phys. Lett. **101**, 183104 (2012).
51. D. DeJarnette, D. K. Roper, and B. Harbin, "Geometric effects on far-field coupling between multipoles of nanoparticles in square arrays," J. Opt. Soc. Am. B **29**, 88–100 (2012).

52. D. DeJarnette, N. Brekke, E. Tunkara, H. Parameswar, K. Roberts, and T. Otanicar, "Design and feasibility of high temperature nanoparticle fluid filter in hybrid thermal/photovoltaic concentrating solar power," Proc. SPIE **9559**, 95590C (2015).
53. T. Jensen, L. Kelly, A. Lazarides, and G. C. Schatz, "Electrodynamics of noble metal nanoparticles and nanoparticle clusters," J. Cluster Sci. **10**, 295–317 (1999).
54. D. DeJarnette, J. Norman, and D. K. Roper, "Attribution of Fano resonant features to plasmonic particle size, lattice constant, and dielectric wavenumber in square nanoparticle lattices," Photon. Res. **2**, 15–23 (2014).
55. C. F. Bohren and D. R. Huffman, *Absorption and Scattering of Light by Small Particles* (Wiley, 1983).
56. S. Ullah, E. P. Ferreira-Neto, A. A. Pasa, C. C. J. Alcantara, J. J. S. Acuna, S. A. Bilmes, M. L. M. Ricci, R. Landers, T. Z. Fermino, and U. P. Rodrigues-Filho, "Enhanced photocatalytic properties of core–shell SiO_2–TiO_2 nanoparticles," Appl. Catal. B **179**, 333–343 (2015).
57. M. Arnold, M. Blaber, and M. Ford, "Local plasmon resonances of metal-in-metal core-shells," Opt. Express **22**, 3186–3198 (2014).
58. A. V. Goncharenko, "Optical properties of core-shell particle composites. I. Linear response," Chem. Phys. Lett. **386**, 25–31 (2004).
59. P. K. Jain, K. S. Lee, I. H. El-Sayed, and M. A. El-Sayed, "Calculated absorption and scattering properties of gold nanoparticles of different size, shape, and composition: applications in biological imaging and biomedicine," J. Phys. Chem. B **110**, 7238–7248 (2006).
60. L. D. Landau and E. M. Lifschitz, *Electrodynamics of Continuous Media*, 2nd ed. (Pergamon, 1984).
61. J. Venermo and A. Sihvola, "Dielectric polarizability of circular cylinder," J. Electrost. **63**, 101–117 (2005).
62. D. DeJarnette, T. Otanicar, N. Brekke, P. Hari, and K. Roberts, "Selective spectral filtration with nanoparticles for concentrating solar collectors," J. Photon. Energy **5**, 057008 (2015).
63. Z.-J. Yang, N.-C. Kim, J.-B. Li, M.-T. Cheng, S.-D. Liu, Z.-H. Hao, and Q.-Q. Wang, "Surface plasmons amplifications in single Ag nanoring," Opt. Express **18**, 4006–4011 (2010).
64. C. Huang, J. Ye, S. Wang, T. Stakenborg, and L. Lagae, "Gold nanoring as a sensitive plasmonic biosensor for on-chip DNA detection," Appl. Phys. Lett. **100**, 173114 (2012).
65. G. T. Forcherio, D. DeJarnette, P. Blake, and D. K. Roper, "Polarizability extraction for rapid computation of Fano resonance in nanoring lattices," Proc. SPIE **9163**, 91633O (2014).
66. H.-Y. Tseng, C.-K. Lee, S.-Y. Wu, T.-T. Chi, K.-M. Yang, J.-Y. Wang, Y.-W. Kiang, C. C. Yang, M.-T. Tsai, Y.-C. Wu, H.-Y. E. Chou, and C.-P. Chiang, "Au nanorings for enhancing absorption and backscattering monitored with optical coherence tomography," Nanotechnology **21**, 295102 (2010).
67. H. Matsui, S. Furuta, and H. Tabata, "Role of electron carriers on local surface plasmon resonances in doped oxide semiconductor nanocrystals," Appl. Phys. Lett. **104**, 211903 (2014).
68. V. Myroshnychenko, J. Rodríguez-Fernández, I. Pastoriza-Santos, A. M. Funston, C. Novo, P. Mulvaney, L. M. Liz-Marzán, and F. J. García de Abajo, "Modelling the optical response of gold nanoparticles," Chem. Soc. Rev. **37**, 1792–1805 (2008).
69. H. Ishihara, K. Cho, K. Akiyama, N. Tomita, Y. Nomura, and T. Isu, "Large four-wave mixing of spatially extended excitonic states in thin GaAs layers," Phys. Rev. Lett. **89**, 017402 (2002).

70. H. Ajiki, T. Tsuji, K. Kawano, and K. Cho, "Optical spectra and exciton-light coupled modes of a spherical semiconductor nanocrystal," Phys. Rev. B **66**, 245322 (2002).
71. K. L. Kelly, E. Coronado, L. L. Zhao, and G. C. Schatz, "The optical properties of metal nanoparticles: the influence of size, shape, and dielectric environment," J. Phys. Chem. B **107**, 668–677 (2003).
72. A. B. Evlyukhin, C. Reinhardt, and B. N. Chichkov, "Multipole light scattering by nonspherical nanoparticles in the discrete dipole approximation," Phys. Rev. B **84**, 235429 (2011).
73. M. Yurkin and A. Hoekstra, "The discrete dipole approximation: an overview and recent developments," J. Quant. Spectrosc. Radiat. Transfer **106**, 558–589 (2007).
74. M. Collinge and B. Draine, "Discrete-dipole approximation with polarizabilities that account for both finite wavelength and target geometry," J. Opt. Soc. Am. A **21**, 2023–2028 (2004).
75. E. Purcell and C. Pennypacker, "Scattering and absorption of light by nonspherical dielectric grains," Astrophys. J. **186**, 705–714 (1973).
76. O. J. F. Martin and N. B. Piller, "Electromagnetic scattering in polarizability backgrounds," Phys. Rev. E **58**, 3909–3915 (1998).
77. R. Filter, M. Farhat, M. Steglich, R. Alaee, C. Rockstuhl, and F. Lederer, "Tunable graphene antennas for selective enhancement of THz-emission," Opt. Express **21**, 3737–3745 (2013).
78. P. Zhao, N. Li, and D. Astruc, "State of the art in gold nanoparticle synthesis," Coord. Chem. Rev. **257**, 638–665 (2013).
79. J. Turkevich, P. C. Stevenson, and J. Hillier, "A study of the nucleation and growth processes in the synthesis of colloidal gold," Discuss. Faraday Soc. **11**, 55–75 (1951).
80. R. Ferrando, J. Jellinek, and R. L. Johnston, "Nanoalloys: from theory to applications of alloy clusters and nanoparticles," Chem. Rev. **108**, 845–910 (2008).
81. A.-H. Lu, E. L. Salabas, and F. Schüth, "Magnetic nanoparticles: synthesis, protection, functionalization, and application," Angew. Chem. Int. Ed. **46**, 1222–1244 (2007).
82. R. G. Chaudhuri and S. Paria, "Core/shell nanoparticles: classes, properties, synthesis mechanisms, characterization, and applications," Chem. Rev. **112**, 2373–2433 (2012).
83. A. Tavakoli, M. Sohrabi, and A. Kargari, "A review of methods for synthesis of nanostructured metals with emphasis on iron compounds," Chem. Pap. **61**, 151–170 (2007).
84. T. Tsuzuki and P. G. McCormick, "Mechanochemical synthesis of nanoparticles," J. Mater. Sci. **39**, 5143–5146 (2004).
85. H. Zeng, X.-W. Du, S. C. Singh, S. A. Kulinich, S. Yang, J. He, and W. Cai, "Nanomaterials via laser ablation/irradiation in liquid: a review," Adv. Funct. Mater. **22**, 1333–1353 (2012).
86. S. Eliezer, N. Eliaz, E. Grossman, D. Fisher, I. Gouzman, Z. Henis, S. Pecker, Y. Horovitz, M. Fraenkel, S. Maman, and Y. Lereah, "Synthesis of nanoparticles with femtosecond laser pulses," Phys. Rev. B **69**, 144119 (2004).
87. Sigma Aldrich, http://www.sigmaaldrich.com/catalog/search?term=Gold+nanoparticles&interface=ProductName&N=0+&mode=modematchpartialmax&lang=en&region=US&focus=productN=022000304821985328621985326 9.
88. NanoComposix, http://nanocomposix.com/collections/dried-gold/products/10-nm-gold-nanospheres.
89. Nanopartz, http://www.nanopartz.com/bare_spherical_gold_nanoparticles.asp.
90. APMEX, http://www.apmex.com/spotprices/gold-price.

91. Y. Xie, L. Carbone, C. Nobile, and V. Grillo, "Metallic-like stoichiometric copper sulfide nanocrystals: phase-and shape-selective synthesis, near-infrared surface plasmon resonance properties, and their modeling," ACS Nano **7**, 7352–7369 (2013).
92. S. D. Lounis, E. L. Runnerstrom, A. Bergerud, D. Nordlund, and D. J. Milliron, "Influence of dopant distribution on the plasmonic properties of indium tin oxide nanocrystals," J. Am. Chem. Soc. **136**, 7110–7116 (2014).
93. M. Kanehara, H. Koike, T. Yoshinaga, and T. Teranishi, "Indium tin oxide nanoparticles with compositionally tunable surface plasmon resonance frequencies in the near-IR region," J. Am. Chem. Soc. **131**, 17736–17737 (2009).
94. G. A. Shah, "Numerical methods for Mie theory of scattering by a sphere," Kodaikanal Obs. Bull. Ser. A **2**, 42–63 (1977).
95. Y.-Y. Yu, S.-S. Chang, C.-L. Lee, and C. R. C. Wang, "Gold nanorods: electrochemical synthesis and optical properties," J. Phys. Chem. B **101**, 6661–6664 (1997).
96. A. Gole and C. Murphy, "Seed-mediated synthesis of gold nanorods: role of the size and nature of the seed," Chem. Mater. **16**, 3633–3640 (2004).
97. D. Weber, P. Albella, P. Alonso-González, F. Neubrech, H. Gui, T. Nagao, R. Hillenbrand, J. Aizpurua, and A. Pucci, "Longitudinal and transverse coupling in infrared gold nanoantenna arrays: long range versus short range interaction regimes," Opt. Express **19**, 15047–15061 (2011).
98. D. DeJarnette, E. Tunkara, N. Brekke, T. Otanicar, K. Roberts, B. Gao, and A. E. Saunders, "Nanoparticle enhanced spectral filtration of insolation from trough concentrators," Sol. Energy Mater. Sol. Cells **149**, 145–153 (2016).
99. C. Guo, S. Yin, Y. Huang, Q. Dong, and T. Sato, "Synthesis of $W_{18}O_{49}$ nanorod via ammonium tungsten oxide and its interesting optical properties," Langmuir **27**, 12172–12178 (2011).
100. C. Guo, S. Yin, L. Huang, L. Yang, and T. Sato, "Discovery of an excellent IR absorbent with a broad working waveband: $Cs_{(x)}WO_3$ nanorods," Chem. Commun. **47**, 8853–8855 (2011).
101. C. Guo, S. Yin, P. Zhang, M. Yan, K. Adachi, T. Chonan, and T. Sato, "Novel synthesis of homogenous Cs_xWO_3 nanorods with excellent NIR shielding properties by a water controlled-release solvothermal process," J. Mater. Chem. **20**, 8227–8229 (2010).
102. R. A. Gilstrap, C. J. Capozzi, C. G. Carson, R. A. Gerhardt, and C. J. Summers, "Synthesis of a nonagglomerated indium tin oxide nanoparticle dispersion," Adv. Mater. **20**, 4163–4166 (2008).
103. S. D. Lounis, E. L. Runnerstrom, A. Llordes, and D. J. Milliron, "Defect chemistry and plasmon physics of colloidal metal oxide nanocrystals," J. Phys. Chem. Lett. **5**, 1564–1574 (2014).
104. H. Takeda, H. Kuno, and K. Adachi, "Solar control dispersions and coatings with rare-earth hexaboride nanoparticles," J. Am. Ceram. Soc. **91**, 2897–2902 (2008).
105. J. M. Luther, P. K. Jain, T. Ewers, and A. P. Alivisatos, "Localized surface plasmon resonances arising from free carriers in doped quantum dots," Nat. Mater. **10**, 361–366 (2011).
106. D. Dorfs, T. Härtling, K. Miszta, N. C. Bigall, M. R. Kim, A. Genovese, A. Falqui, M. Povia, and L. Manna, "Reversible tunability of the near-infrared valence band plasmon resonance in $Cu_{(2-x)}Se$ nanocrystals," J. Am. Chem. Soc. **133**, 11175–11180 (2011).
107. B. Rodríguez-González, A. Burrows, M. Watanabe, C. J. Kiely, and L. M. Liz-Marzán, "Multishell bimetallic AuAg nanoparticles: synthesis, structure and optical properties," J. Mater. Chem. **15**, 1755–1759 (2005).

108. R. Jiang, B. Li, C. Fang, and J. Wang, "Metal/semiconductor hybrid nanostructures for plasmon-enhanced applications," Adv. Mater. **26**, 5274–5309 (2014).
109. D. DeJarnette, P. Blake, G. T. Forcherio, and D. Keith Roper, "Far-field Fano resonance in nanoring lattices modeled from extracted, point dipole polarizability," J. Appl. Phys. **115**, 024306 (2014).
110. C. L. Nehl, H. Liao, and J. H. Hafner, "Optical properties of star-shaped gold nanoparticles," Nano Lett. **6**, 683–688 (2006).
111. H. Chen, X. Kou, Z. Yang, W. Ni, and J. Wang, "Shape- and size-dependent refractive index sensitivity of gold nanoparticles," Langmuir **24**, 5233–5237 (2008).
112. P. Nordlander, C. Oubre, E. Prodan, K. Li, and M. I. Stockman, "Plasmon hybridization in nanoparticle dimers," Nano Lett. **4**, 899–903 (2004).
113. F. B. Arango, T. Coenen, and A. Koenderink, "Underpinning hybridization intuition for complex nanoantennas by magnetoelectric quadrupolar polarizability retrieval," ACS Photon. **1**, 444–453 (2014).
114. A. L. Koh, K. Bao, I. Khan, W. E. Smith, G. Kothleitner, P. Nordlander, S. A. Maier, and D. W. McComb, "Electron energy-loss spectroscopy (EELS) of surface plasmons in single silver nanoparticles and dimers: influence of beam damage and mapping of dark modes," ACS Nano **3**, 3015–3022 (2009).
115. C. David and F. J. García de Abajo, "Spatial nonlocality in the optical response of metal nanoparticles," J. Phys. Chem. C **115**, 19470–19475 (2011).
116. W. De Rooij and C. van der Stap, "Expansion of Mie scattering matrices in generalized spherical functions," Astron. Astrophys. **131**, 237–248 (1984).
117. A. Monti, A. Alù, A. Toscano, and F. Bilotti, "Optical invisibility through metasurfaces made of plasmonic nanoparticles," J. Appl. Phys. **117**, 123103 (2015).
118. S. Link and M. El-Sayed, "Spectral properties and relaxation dynamics of surface plasmon electronic oscillations in gold and silver nanodots and nanorods," J. Phys. Chem. B **103**, 8410–8426 (1999).
119. D. DeJarnette, G. G. Jang, P. Blake, and D. K. Roper, "Polarization angle affects energy of plasmonic features in Fano resonant regular lattices," J. Opt. **16**, 105006 (2014).
120. H. Mertens, J. S. Biteen, H. A. Atwater, and A. Polman, "Polarization-selective plasmon-enhanced silicon quantum-dot luminescence," Nano Lett. **6**, 2622–2625 (2006).
121. G. T. Forcherio, P. Blake, D. DeJarnette, and D. K. Roper, "Nanoring structure, spacing, and local dielectric sensitivity for plasmonic resonances in Fano resonant square lattices," Opt. Express **22**, 17791–17804 (2014).
122. J. Nelayah, M. Kociak, O. Stéphan, N. Geuquet, L. Henrard, F. J. García de Abajo, I. Pastoriza-Santos, L. M. Liz-Marzán, and C. Colliex, "Two-dimensional quasistatic stationary short range surface plasmons in flat nanoprisms," Nano Lett. **10**, 902–907 (2010).
123. B. Pietrobon and V. Kitaev, "Photochemical synthesis of monodisperse size-controlled silver decahedral nanoparticles and their remarkable optical properties," Chem. Mater. **20**, 5186–5190 (2008).
124. M. W. Knight and N. J. Halas, "Nanoshells to nanoeggs to nanocups: optical properties of reduced symmetry core-shell nanoparticles beyond the quasistatic limit," New J. Phys. **10**, 105006 (2008).
125. J. B. Lassiter, M. W. Knight, N. A. Mirin, and N. J. Halas, "Reshaping the plasmonic properties of an individual nanoparticle," Nano Lett. **9**, 4326–4332 (2009).
126. C. Ayala-Orozco, J. G. Liu, M. W. Knight, Y. Wang, J. K. Day, P. Nordlander, and N. J. Halas, "Fluorescence enhancement of molecules inside a gold nanomatryoshka," Nano Lett. **14**, 2926–2933 (2014).

127. S. E. Skrabalak, J. Chen, Y. Sun, X. Lu, L. Au, C. M. Cobley, and Y. Xia, "Gold nanocages: synthesis, properties, and applications," Acc. Chem. Res. **41**, 1587–1595 (2008).
128. Y. Xiang, X. Wu, D. Liu, Z. Li, W. Chu, L. Feng, K. Zhang, W. Zhou, and S. Xie, "Gold nanorod-seeded growth of silver nanostructures: from homogeneous coating to anisotropic coating," Langmuir **24**, 3465–3470 (2008).
129. S. Kumar and C. L. Tien, "Dependent absorption and extinction of radiation by small particles," J. Heat Transfer **112**, 178–185 (1990).
130. O. Kulakovich, N. Strekal, A. Yaroshevich, S. Maskevich, S. Gaponenko, I. Nabiev, U. Woggon, and M. Artemyev, "Enhanced luminescence of CdSe quantum dots on gold colloids," Nano Lett. **2**, 1449–1452 (2002).
131. Z. Li, L. Wang, Z. Wang, X. Liu, and Y. Xiong, "Modification of $NaYF_4$:Yb, Er–SiO_2 nanoparticles with gold nanocrystals for tunable green-to-red upconversion emissions," J. Phys. Chem. C **115**, 3291–3296 (2011).
132. W. Lv, P. E. Phelan, R. Swaminathan, T. P. Otanicar, and R. A. Taylor, "Multifunctional core-shell nanoparticle suspensions for efficient absorption," J. Sol. Energy Eng. **135**, 021004 (2013).
133. C. Telang, T. Otanicar, L. Dai, P. Phelan, R. Swaminathan, and M. Zhang, "Controllable optical properties of polystyrene/PNIPAM-gold composite nanoparticles," Plasmonics **10**, 17–25 (2015).
134. D. Suzuki and H. Kawaguchi, "Hybrid microgels with reversibly changeable multiple brilliant color," Langmuir **22**, 3818–3822 (2006).
135. H. Xu and M. Käll, "Surface-plasmon-enhanced optical forces in silver nanoaggregates," Phys. Rev. Lett. **89**, 246802 (2002).
136. A. J. Hallock, P. L. Redmond, and L. E. Brus, "Optical forces between metallic particles," Proc. Natl. Acad. Sci. USA **102**, 1280–1284 (2005).
137. T. Iida, "Control of plasmonic superradiance in metallic nanoparticle assembly by light-induced force and fluctuations," J. Phys. Chem. Lett. **3**, 332–336 (2012).
138. S. Tokonami, S. Hidaka, K. Nishida, Y. Yamamoto, H. Nakao, and T. Iida, "Multipole superradiance from densely assembled metallic nanoparticles," J. Phys. Chem. B **117**, 15247–15252 (2013).
139. T. Atay, J.-H. Song, and A. V. Nurmikko, "Strongly interacting plasmon nanoparticle pairs: from dipole-dipole interaction to conductively coupled regime," Nano Lett. **4**, 1627–1631 (2004).
140. K.-H. Su, Q.-H. Wei, X. Zhang, J. J. Mock, D. R. Smith, and S. Schultz, "Interparticle coupling effects on plasmon resonances of nanogold particles," Nano Lett. **3**, 1087–1090 (2003).
141. W. Rechberger, A. Hohenau, A. Leitner, J. R. Krenn, B. Lamprecht, and F. R. Aussenegg, "Optical properties of two interacting gold nanoparticles," Opt. Commun. **220**, 137–141 (2003).
142. B. Auguié and W. L. Barnes, "Collective resonances in gold nanoparticle arrays," Phys. Rev. Lett. **101**, 143902 (2008).
143. C. L. Haynes, A. D. McFarland, L. Zhao, R. P. Van Duyne, and G. C. Schatz, "Nanoparticle optics: the importance of radiative dipole coupling in two-dimensional nanoparticle arrays," J. Phys. Chem. B **107**, 7337–7342 (2003).
144. R. Looser, M. Vivar, and V. Everett, "Spectral characterisation and long-term performance analysis of various commercial heat transfer fluids (HTF) as direct-absorption filters for CPV-T beam-splitting applications," Appl. Energy **113**, 1496–1511 (2014).
145. W. A. M. Al-Shohani, A. Sabouri, R. Al-Dadah, S. Mahmoud, and H. Butt, "Experimental investigation of an optical water filter for photovoltaic/thermal conversion module," Energy Convers. Manag. **111**, 431–442 (2016).

146. S. S. Joshi, A. S. Dhoble, and P. R. Jiwanapurkar, "Investigations of different liquid based spectrum beam splitters for combined solar photovoltaic thermal systems," J. Sol. Energy Eng. **138**, 021003 (2016).
147. A. Mojiri, C. Stanley, and G. Rosengarten, "A high temperature hybrid photovoltaic-thermal receiver employing spectral beam splitting for linear solar concentrators," Proc. SPIE **9559**, 95590D (2015).
148. S. Vijayaraghavan, S. Ganapathisubbu, and C. Santosh Kumar, "Performance analysis of a spectrally selective concentrating direct absorption collector," Sol. Energy **97**, 418–425 (2013).
149. T. P. Otanicar, I. Chowdhury, R. Prasher, and P. E. Phelan, "Band-gap tuned direct absorption for a hybrid concentrating solar photovoltaic/thermal system," J. Sol. Energy Eng. **133**, 041014 (2011).
150. R. A. Taylor, T. P. Otanicar, and G. Rosengarten, "Nanofluid-based optical filter optimization for PV/T systems," Light Sci. Appl. **1**, e34 (2012).
151. R. A. Taylor, T. P. Otanicar, Y. Herukerrupu, F. Bremond, G. Rosengarten, E. R. Hawkes, X. Jiang, and S. Coulombe, "Feasibility of nanofluid-based optical filters," Appl. Opt. **52**, 1413–1422 (2013).
152. N. E. Hjerrild, S. Mesgari, F. Crisostomo, J. A. Scott, R. Amal, and R. A. Taylor, "Hybrid PV/T enhancement using selectively absorbing Ag-SiO_2/carbon nanofluids," Sol. Energy Mater. Sol. Cells **147**, 281–287 (2016).
153. W. An, J. Zhang, T. Zhu, and N. Gao, "Investigation on a spectral splitting photovoltaic/thermal hybrid system based on polypyrrole nanofluid: preliminary test," Renew. Energy **86**, 633–642 (2016).
154. D. Jing, Y. Hu, M. Liu, J. Wei, and L. Guo, "Preparation of highly dispersed nanofluid and CFD study of its utilization in a concentrating PV/T system," Sol. Energy **112**, 30–40 (2015).
155. N. Brekke, T. Otanicar, D. DeJarnette, and P. Harikumar, "A parametric investigation of a concentrating PV/T system with spectral filtering utilizing a 2-D heat transfer model," J. Sol. Energy Eng. **138**, 021007 (2016).
156. R. Wolf, H. Matz, E. Orion, and J. Lipozencić, "Sunscreens—the ultimate cosmetic," Acta Dermatovenerol. Croat. **11**, 158–162 (2003).
157. T. G. Smijs and S. Pavel, "Titanium dioxide and zinc oxide nanoparticles in sunscreens: focus on their safety and effectiveness," Nanotechnol. Sci. Appl. **4**, 95–112 (2011).
158. T. Kaida, K. Kobayashi, M. Adachi, and F. Suzuki, "Optical characteristics of titanium oxide interference film and the film laminated with oxides and their applications for cosmetics," J. Cosmet. Sci. **55**, 219–220 (2004).
159. M. J. Mendes, S. Morawiec, T. Mateus, A. Lyubchyk, H. Águas, I. Ferreira, E. Fortunato, R. Martins, F. Priolo, and I. Crupi, "Broadband light trapping in thin film solar cells with self-organized plasmonic nano-colloids," Nanotechnology **26**, 135202 (2015).
160. X. Hua, Z. Zhou, L. Yuan, and S. Liu, "Selective collection and detection of MCF-7 breast cancer cells using aptamer-functionalized magnetic beads and quantum dots based nano-bio-probes," Anal. Chim. Acta **788**, 135–140 (2013).
161. L.-D. Sun, Y.-F. Wang, and C.-H. Yan, "Paradigms and challenges for bioapplication of rare earth upconversion luminescent nanoparticles: small size and tunable emission/excitation spectra," Acc. Chem. Res. **47**, 1001–1009 (2014).
162. K. Welsher, Z. Liu, D. Daranciang, and H. Dai, "Selective probing and imaging of cells with single walled carbon nanotubes as near-infrared fluorescent molecules," Nano Lett. **8**, 586–590 (2008).
163. J. M. Dubach, D. I. Harjes, and H. A. Clark, "Ion-selective nano-optodes incorporating quantum dots," J. Am. Chem. Soc. **129**, 8418–8419 (2007).

164. Y. Masuda, N. Kinoshita, F. Sato, and K. Koumoto, "Site-selective deposition and morphology control of UV- and visible-light-emitting ZnO crystals," Cryst. Growth Des. **6**, 75–78 (2006).
165. Z. Xu, X. Kang, C. Li, Z. Hou, C. Zhang, D. Yang, G. Li, and J. Lin, "Ln^{3+} (Ln = Eu, Dy, Sm, and Er) ion-doped YVO_4 nano/microcrystals with multiform morphologies: hydrothermal synthesis, growing mechanism, and luminescent properties," Inorg. Chem. **49**, 6706–6715 (2010).
166. M. Tschikin, S.-A. Biehs, F. S. S. Rosa, and P. Ben-Abdallah, "Radiative cooling of nanoparticles close to a surface," Eur. Phys. J. B **85**, 233 (2012).
167. T. P. Otanicar, "Enhancing the heat transfer in energy systems from a volumetric approach," in *ASME/JSME 8th Thermal Engineering Joint Conference*, Honolulu, Hawaii, USA, 13–17 March 2011, paper T30074.
168. T. P. Otanicar, R. Smith, L. Dai, P. E. Phelan, and R. Swaminathan, "Applicability of controllable nanoparticle radiative properties for spacecraft heat rejection," J. Thermophys. Heat Transfer **29**, 869–874 (2015).
169. C. Guo, S. Yin, M. Yan, M. Kobayashi, M. Kakihana, and T. Sato, "Morphology-controlled synthesis of $W_{18}O_{49}$ nanostructures and their near-infrared absorption properties," Inorg. Chem. **51**, 4763–4771 (2012).
170. K. Adachi and T. Asahi, "Activation of plasmons and polarons in solar control cesium tungsten bronze and reduced tungsten oxide nanoparticles," J. Mater. Res. **27**, 965–970 (2012).
171. C. Guo, S. Yin, L. Huang, and T. Sato, "Synthesis of one-dimensional potassium tungsten bronze with excellent near-infrared absorption property," ACS Appl. Mater. Interfaces **3**, 2794–2799 (2011).
172. N. DeForest, A. Shehabi, J. O'Donnell, G. Garcia, J. Greenblatt, E. S. Lee, S. Selkowitz, and D. J. Milliron, "United States energy and CO_2 savings potential from deployment of near-infrared electrochromic window glazings," Build. Environ. **89**, 107–117 (2015).
173. S.-Y. Li, G. A. Niklasson, and C. G. Granqvist, "Nanothermochromics: calculations for VO_2 nanoparticles in dielectric hosts show much improved luminous transmittance and solar energy transmittance modulation," J. Appl. Phys. **108**, 063525 (2010).
174. E. L. Runnerstrom, A. Llordés, S. D. Lounis, and D. J. Milliron, "Nanostructured electrochromic smart windows: traditional materials and NIR-selective plasmonic nanocrystals," Chem. Commun. **50**, 10555–10572 (2014).
175. G. Garcia, R. Buonsanti, E. L. Runnerstrom, R. J. Mendelsberg, A. Llordes, A. Anders, T. J. Richardson, and D. J. Milliron, "Dynamically modulating the surface plasmon resonance of doped semiconductor nanocrystals," Nano Lett. **11**, 4415–4420 (2011).
176. A. Agrawal, I. Kriegel, and D. J. Milliron, "Shape-dependent field enhancement and plasmon resonance of oxide nanocrystals," J. Phys. Chem. C **119**, 6227–6238 (2015).
177. R. Buonsanti, A. Llordes, S. Aloni, B. A. Helms, and D. J. Milliron, "Tunable infrared absorption and visible transparency of colloidal aluminum-doped zinc oxide nanocrystals," Nano Lett. **11**, 4706–4710 (2011).
178. R. A. Taylor, T. P. Otanicar, Y. L. Hewakuruppu, and D. DeJarnette, "Comparison of selective transmitters for solar thermal applications," Appl. Opt. **55**, 3829–3839 (2016).
179. J. Li, X. Hu, Y. Gu, and Q. Gong, "Tunable wavelength-division multiplexing based on metallic nanoparticle arrays," Opt. Lett. **35**, 4051–4053 (2010).
180. L. Zhao, K. L. Kelly, and G. C. Schatz, "The extinction spectra of silver nanoparticle arrays: influence of array structure on plasmon resonance wavelength and width," J. Phys. Chem. B **107**, 7343–7350 (2003).

181. D. K. Roper, W. Ahn, B. Taylor, and A. G. Dall'Asén, "Enhanced spectral sensing by electromagnetic coupling with localized surface plasmons on subwavelength structures," IEEE Sens. J. **10**, 531–540 (2010).
182. V. Giannini, Y. Francescato, H. Amrania, C. C. Phillips, and S. A. Maier, "Fano resonances in nanoscale plasmonic systems: a parameter-free modeling approach," Nano Lett. **11**, 2835–2840 (2011).
183. W. Barnes, A. Dereux, and T. Ebbesen, "Surface plasmon subwavelength optics," Nature **424**, 824–830 (2003).
184. P. Spinelli, V. E. Ferry, J. van de Groep, M. van Lare, M. A. Verschuuren, R. E. I. Schropp, H. A. Atwater, and A. Polman, "Plasmonic light trapping in thin-film Si solar cells," J. Opt. **14**, 024002 (2012).
185. H. A. Atwater and A. Polman, "Plasmonics for improved photovoltaic devices," Nat. Mater. **9**, 205–213 (2010).
186. E. L. I. Yablonovitch and G. D. Cody, "Intensity enhancement in textured optical sheets for solar cells," IEEE Trans. Electron Devices **29**, 300–305 (1982).
187. F. J. Beck, A. Polman, K. R. Catchpole, F. J. Beck, A. Polman, and K. R. Catchpole, "Tunable light trapping for solar cells using localized surface plasmons," J. Appl. Phys. **105**, 114310 (2009).
188. J. Zhao, A. Wang, M. A. Green, and F. Ferrazza, "19.8% efficient 'honeycomb' textured multicrystalline and 24.4% monocrystalline silicon solar cells," Appl. Phys. Lett. **73**, 1991–1993 (1998).
189. P. Campbell, M. A. Green, P. Campbell, and M. A. Green, "Light trapping properties of pyramidally textured surfaces," J. Appl. Phys. **62**, 243–249 (1987).
190. C. Van Lare, F. Lenzmann, M. A. Verschuuren, and A. Polman, "Dielectric scattering patterns for efficient light trapping in thin-film solar cells," Nano Lett. **15**, 4846–4852 (2015).
191. C. F. Guo, T. Sun, F. Cao, Q. Liu, and Z. Ren, "Metallic nanostructures for light trapping in energy-harvesting devices," Light Sci. Appl. **3**, e161 (2016).
192. J. G. Smith, J. A. Faucheaux, and P. K. Jain, "Plasmon resonances for solar energy harvesting: a mechanistic outlook," Nano Today **10**(1), 67–80 (2015).
193. A. W. Powell, M. B. Wincott, A. A. R. Watt, H. E. Assender, and J. M. Smith, "Controlling the optical scattering of plasmonic nanoparticles using a thin dielectric layer," J. Appl. Phys. **113**, 184311 (2013).
194. R. S. A. Sesuraj, T. L. Temple, and D. M. Bagnall, "Optical characterisation of a spectrally tunable plasmonic reflector for application in thin-film silicon solar cells," Sol. Energy Mater. Sol. Cells **111**, 23–30 (2013).
195. F. J. Beck, S. Mokkapati, and K. R. Catchpole, "Plasmonic light-trapping for Si solar cells using self-assembled, Ag nanoparticles," Prog. Photovolt. Res. Appl. **18**, 500–504 (2010).
196. H. Tan, R. Santbergen, A. H. M. Smets, and M. Zeman, "Plasmonic light trapping in thin-film silicon solar cells with improved self-assembled silver nanoparticles," Nano Lett. **12**, 4070–4076 (2012).
197. F. C. Chen, J. L. Wu, C. L. Lee, Y. Hong, C. H. Kuo, and M. H. Huang, "Plasmonic-enhanced polymer photovoltaic devices incorporating solution-processable metal nanoparticles," Appl. Phys. Lett. **95**, 2012–2015 (2009).
198. M. J. Mendes, S. Morawiec, F. Simone, F. Priolo, and I. Crupi, "Colloidal plasmonic back reflectors for light trapping in solar cells," Nanoscale **6**, 4796–4805 (2014).
199. H. Shen, P. Bienstman, and B. Maes, "Plasmonic absorption enhancement in organic solar cells with thin active layers," J. Appl. Phys. **106**, 073109 (2009).

200. J.-Y. Lee and P. Peumans, "The origin of enhanced optical absorption in solar cells with metal nanoparticles embedded in the active layer," Opt. Express **18**, 10078–10087 (2010).
201. A. Dabirian and N. Taghavinia, "Theoretical study of light trapping in nanostructured thin film solar cells using wavelength-scale silver particles," ACS Appl. Mater. Interface **7**, 14926–14932 (2015).
202. S.-S. Kim, S.-I. Na, J. Jo, D.-Y. Kim, and Y.-C. Nah, "Plasmon enhanced performance of organic solar cells using electrodeposited Ag nanoparticles," Appl. Phys. Lett. **93**, 073307 (2008).
203. Y. Zhang, Z. Ouyang, N. Stokes, B. Jia, Z. Shi, and M. Gu, "Low cost and high performance Al nanoparticles for broadband light trapping in Si wafer solar cells," Appl. Phys. Lett. **100**, 151101 (2012).
204. X. Chen, B. Jia, Y. Zhang, and M. Gu, "Exceeding the limit of plasmonic light trapping in textured screen-printed solar cells using Al nanoparticles and wrinkle-like graphene sheets," Light Sci. Appl. **2**, e92 (2013).
205. J. R. C. Smirnov, M. E. Calvo, and H. Míguez, "Selective UV reflecting mirrors based on nanoparticle multilayers," Adv. Funct. Mater. **23**, 2805–2811 (2013).
206. P. G. O'Brien, Y. Yang, A. Chutinan, P. Mahtani, K. Leong, D. P. Puzzo, L. D. Bonifacio, C.-W. Lin, G. A. Ozin, and N. P. Kherani, "Selectively transparent and conducting photonic crystal solar spectrum splitters made of alternating sputtered indium-tin oxide and spin-coated silica nanoparticle layers for enhanced photovoltaics," Sol. Energy Mater. Sol. Cells **102**, 173–183 (2012).
207. M. D. Ooms, Y. Jeyaram, and D. Sinton, "Wavelength-selective plasmonics for enhanced cultivation of microalgae," Appl. Phys. Lett. **106**, 063902 (2015).
208. S. Torkamani, S. N. Wani, Y. J. Tang, and R. Sureshkumar, "Plasmon-enhanced microalgal growth in miniphotobioreactors," Appl. Phys. Lett. **97**, 043703 (2010).
209. B. Estime, D. Ren, and R. Sureshkumar, "Effects of plasmonic film filters on microalgal growth and biomass composition," Algal Res. **11**, 85–89 (2015).
210. E. Eroglu, P. K. Eggers, M. Winslade, S. M. Smith, and C. L. Raston, "Enhanced accumulation of microalgal pigments using metal nanoparticle solutions as light filtering devices," Green Chem. **15**, 3155–3159 (2013).
211. T. M. J. Nilsson and G. A. Niklasson, "Radiative cooling during the day: simulations and experiments on pigmented polyethylene cover foils," Sol. Energy Mater. Sol. Cells **37**, 93–118 (1995).
212. A. R. Gentle and G. B. Smith, "Radiative heat pumping from the Earth using surface phonon resonant nanoparticles," Nano Lett. **10**, 373–379 (2010).
213. A. Ghanekar, L. Lin, J. Su, H. Sun, and Y. Zheng, "Role of nanoparticles in wavelength selectivity of multilayered structures in the far-field and near-field regimes," Opt. Express **23**, A1129–A1139 (2015).
214. W. Van Sark, "Luminescent solar concentrators—a low cost photovoltaics alternative," in *EPJ Web of Conferences* (2012), Vol. **33**, paper 02003–1.
215. R. Kinderman, L. H. Slooff, A. R. Burgers, N. J. Bakker, A. Büchtemann, R. Danz, and J. A. M. van Roosmalen, "I-V performance and stability study of dyes for luminescent plate concentrators," J. Sol. Energy Eng. **129**, 277–282 (2007).
216. W. B. Choi, Y. W. Jin, H. Y. Kim, S. J. Lee, M. J. Yun, J. H. Kang, Y. S. Choi, N. S. Park, and N. S. Lee, "Electrophoresis deposition of carbon nanotubes for triode-type field emission display," Appl. Phys. Lett. **1547**, 41–44 (2012).
217. J. I. Sohn, S. Lee, Y.-H. Song, S.-Y. Choi, K.-I. Cho, and K.-S. Nam, "Patterned selective growth of carbon nanotubes and large field emission from vertically well-aligned carbon nanotube field emitter arrays," Appl. Phys. Lett. **78**, 901–903 (2001).

218. L. Chen, H. Yu, J. Zhong, C. Wu, L. Hu, and T. Zhang, "Effectively improved field emission properties of multiwalled carbon nanotubes/graphenes composite field emitter by covering on the Si pyramidal structure," IEEE Trans. Electron Devices **62**, 4305–4312 (2015).
219. D. Nawn, D. Banerjee, and K. K. Chattopadhyay, "Zinc oxide nanostructure decorated amorphous carbon nanotubes: an improved field emitter," Diam. Relat. Mater. **34**, 50–59 (2013).
220. H. Zeng, W. Cai, P. Liu, X. Xu, H. Zhou, C. Klingshirn, and H. Kalt, "ZnO-based hollow nanoparticles by selective etching: elimination and reconstruction of metal-semiconductor interface, improvement of blue emission and photocatalysis," ACS Nano **2**, 1661–1670 (2008).
221. J. R. Riley, S. Padalkar, Q. Li, P. Lu, D. D. Koleske, J. J. Wierer, G. T. Wang, and L. J. Lauhon, "Three-dimensional mapping of quantum wells in a GaN/InGaN core–shell nanowire light-emitting diode array," Nano Lett. **13**, 4317–4325 (2013).
222. H. Delavari Amrei, R. Ranjbar, S. Rastegar, B. Nasernejad, and A. Nejadebrahim, "Using fluorescent material for enhancing microalgae growth rate in photobioreactors," J. Appl. Phycol. **27**, 67–74 (2015).
223. L. Wondraczek, M. Batentschuk, M. A. Schmidt, R. Borchardt, S. Scheiner, B. Seemann, P. Schweizer, and C. J. Brabec, "Solar spectral conversion for improving the photosynthetic activity in algae reactors," Nat. Commun. **4**, 2047 (2013).
224. L. Wondraczek, E. Tyystjärvi, J. Méndez-Ramos, F. A. Müller, and Q. Zhang, "Shifting the sun: solar spectral conversion and extrinsic sensitization in natural and artificial photosynthesis," Adv. Sci. **2**, 1500218 (2015).
225. J. Chen and J. X. Zhao, "Upconversion nanomaterials: synthesis, mechanism, and applications in sensing," Sensors **12**, 2414–2435 (2012).
226. M. Wang, G. Abbineni, A. Clevenger, C. Mao, and S. Xu, "Upconversion nanoparticles: synthesis, surface modification and biological applications," Nanomedicine **7**, 710–729 (2011).
227. M. Haase and H. Schäfer, "Upconverting nanoparticles," Angew. Chem. Int. Ed. **50**, 5808–5829 (2011).
228. N. Chong and L. Wong, "Algal purification system with efficient solar light utilization," U.S. patent 7,985,338 B1 (July 26, 2011).
229. C. Clavero, "Plasmon-induced hot-electron generation at nanoparticle/metal-oxide interfaces for photovoltaic and photocatalytic devices," Nat. Photonics **8**, 95–103 (2014).
230. Z. Fang, Z. Liu, Y. Wang, P. M. Ajayan, P. Nordlander, and N. J. Halas, "Graphene-antenna sandwich photodetector," Nano Lett. **12**, 3808–3813 (2012).
231. A. Hoggard, L.-Y. Wang, L. Ma, Y. Fang, G. You, J. Olson, Z. Liu, W.-S. Chang, P. M. Ajayan, and S. Link, "Using the plasmon linewidth to calculate the time and efficiency of electron transfer between gold nanorods and graphene," ACS Nano **7**, 11209–11217 (2013).
232. I. Robel, V. Subramanian, M. Kuno, and P. V. Kamat, "Quantum dot solar cells. Harvesting light energy with CdSe nanocrystals molecularly linked to mesoscopic TiO_2 films," J. Am. Chem. Soc. **128**, 2385–2393 (2006).
233. I. Robel, M. Kuno, and P. V. Kamat, "Size-dependent electron injection from excited CdSe quantum dots into TiO_2 nanoparticles," J. Am. Chem. Soc. **129**, 4136–4137 (2007).
234. M. C. Beard, K. P. Knutsen, P. Yu, J. M. Luther, Q. Song, W. K. Metzger, R. J. Ellingson, and A. J. Nozik, "Multiple exciton generation in colloidal silicon nanocrystals," Nano Lett. **7**, 2506–2512 (2007).

235. T. P. Otanicar, R. A. Taylor, and C. Telang, "Photovoltaic/thermal system performance utilizing thin film and nanoparticle dispersion based optical filters," J. Renewable Sustainable Energy **5**, 033124 (2013).
236. K. Manthiram and A. P. Alivisatos, "Tunable localized surface plasmon resonances in tungsten oxide nanocrystals," J. Am. Chem. Soc. **134**, 3995–3998 (2012).

Todd Otanicar received his Ph.D. in 2009 from Arizona State University in Mechanical Engineering. Todd's research interests are on the dynamic and passive control of mass and heat transport utilizing nanotechnology. His work has been applied in solar collectors, space radiators, and water purification. among others. He is a Licensed Professional Engineer in the state of Oklahoma.

Drew DeJarnette received his Ph.D. in 2014 from the University of Arkansas in Microelectronics Photonics. His research has been focused on the control and manipulation of light using nanoscale materials and devices. He has developed technologies regarding nanoscale sensors in radiation, theranostics, and nanofilters in solar energy.

Dr. Yasitha Hewakuruppu completed his Ph.D. at UNSW-Australia in 2016 and his bachelor's at the University of Sydney in 2011, both in Mechanical Engineering. His research interests are in optics, solar, energy, and nanotechnology. He currently works at Ericsson-Australia as a Telecommunication Engineer and is enjoying his time in the industry.

Robert A. Taylor received his Ph.D. in 2011 from Arizona State University in the School for Engineering of Matter, Transport, and Energy. Dr. Taylor's main research interest is in the development of "next-generation" solar thermal collectors. Drawing on the fields of heat transfer and nanotechnology, he is researching new/novel working fluids and materials for solar systems.